

# CM<sup>2</sup> MAGAZINE



第 43 期



南方科技大学海洋磁学中心主编

## 创刊词

海洋是生命的摇篮，是文明的纽带。地球上最早的生命诞生于海洋，海洋里的生命最终进化成了人类，人类的文化融合又通过海洋得以实现。人因海而兴。

人类对海洋的探索从未停止。从远古时代美丽的神话传说，到麦哲伦的全球航行，再到现代对大洋的科学钻探计划，海洋逐渐从人类敬畏崇拜幻想的精神寄托演变成可以开发利用与科学的研究的客观存在。其中，上个世纪与太空探索同步发展的大洋科学钻探计划将人类对海洋的认知推向了崭新的纬度：深海（deep sea）与深时（deep time）。大洋钻探计划让人类知道，奔流不息的大海之下，埋藏的却是亿万年的地球历史。它们记录了地球板块的运动，从而使板块构造学说得到证实；它们记录了地球环境的演变，从而让古海洋学方兴未艾。

在探索海洋的悠久历史中，从大航海时代的导航，到大洋钻探计划中不可或缺的磁性地层学，磁学发挥了不可替代的作用。这不是偶然，因为从微观到宏观，磁性是最基本的物理属性之一，可以说，万物皆有磁性。基于课题组的学科背景和对海洋的理解，我们对海洋的探索以磁学为主要手段，海洋磁学中心因此而生。

海洋磁学中心，简称 CM<sup>2</sup>，一为其全名“Centre for Marine Magnetism”的缩写，另者恰与爱因斯坦著名的质能方程  $E=MC^2$  对称，借以表达我们对科学巨匠的敬仰和对科学的不懈追求。

然而科学从来不是单打独斗的产物。我们以磁学为研究海洋的主攻利器，但绝不仅限于磁学。凡与磁学相关的领域均是我们关注的重点。为了跟踪反映国内外地球科学特别是与磁学有关的地球科学领域的最新研究进展，海洋磁学中心特地主办 CM<sup>2</sup> Magazine，以期与各位地球科学工作者相互交流学习、合作共进！

“海洋孕育了生命，联通了世界，促进了发展”。21 世纪是海洋科学的时代，由陆向海，让我们携手迈进中国海洋科学的黄金时代！

## 目录

研究进展 .....	1
JGR: 东亚早三叠世古地理 .....	1
ESR: 中布容气候两阶段转型及其对中更新世人类分异演化的环境调控 .....	4
岩石磁学演绎 .....	7
第 33 章 磁学性质的温度效应参数总结.....	7
文献速递 .....	11
1. 侏罗纪早期大洋缺氧事件时期碳释放和风化作用直接相关.....	11
2. 在 OAE2 期间海洋有机碳埋藏增加森林大火频率 .....	14
3. 地幔过渡带内滞留的板片前缘控制着东北亚地区新生代陆内高镁安山岩的形成.....	17
4. 揭示 Powell 海盆的构造域和异常的磁异常特征 .....	19
5. 超越二阶磁各向异性的张量: 辉石中定向磁铁矿析出导致的更高阶分量及其对古磁和构造解释的意义.....	22
6. 河流流量变化与气候和河流扇形成之间的关系.....	24
7. 东非裂谷系统运动学的重新定义.....	27
8. 磁铁矿磁小体的热稳定性: 对化石记录和生物技术的启示 .....	29
9. 新仙女木冷事件气候模型模拟对比.....	31
10. 中更新世气候过渡期中国古人类的分布和行为.....	33
11. 上新世北半球冰盖因大西洋径向翻转流的增强而扩大.....	36
12. 非稳态成岩作用下自生亚铁磁性硫化铁的保存 .....	40

## 研究进展

### JGR: 东亚早三叠世古地理

中生代是潘吉亚超大陆裂解到亚洲大陆形成的关键时期。随着晚古生代中亚造山带的演化，华北、蒙古、塔里木等块体拼合形成现今亚洲大陆的雏形，可称之为原亚洲大陆(Proto-Asia)。早中生代原亚洲大陆与北部西伯利亚板块以蒙古-鄂霍茨克洋相隔，与南部华南、羌塘等块体以古特提斯洋分开。因此，原亚洲大陆位置的准确确定是影响整个东亚中生代古地理重建的重要因素。

华北克拉通作为原亚洲大陆的核心块体，中生代盆地以红色碎屑沉积为主，早期古地磁研究较少考虑磁倾角浅化带来的影响，导致华北板块的古纬度偏低和古地磁极的偏差，并进一步对区域构造以及古地理重建产生影响。另外，前人早三叠世古地磁结果集中于华北克拉通西部，缺乏对东部的研究。华北克拉通中生代经历多期次构造事件影响，来自不同方向的应力使华北克拉通内部发育多个后期大型走滑断裂（图 1），这些走滑断裂是否会影响华北克拉通的整体性，需要针对性研究。

针对以上问题，中科院地质与地球物理研究所赵盼副研究员与德国图宾根大学 Erwin Appel 教授和北京大学徐备教授合作，选取华北北缘中生代承德盆地早三叠世红色砂岩开展古地磁研究，以期确定中生代盆地的倾角浅化程度，并讨论东亚各块体早中生代古地理格局。结果显示：

(1) 承德盆地早三叠世红色砂岩存在显著磁倾角浅化，采用 E/I 方法获得浅化因子  $f = 0.48$ 。

(2) 对比显示，华北克拉通东部和西部古地磁结果一致（图 2），华北克拉通整体性未受后期构造运动，特别是走滑断裂的影响。

(3) 华北克拉通与西伯利亚和华南在早三叠世存在大角度磁偏角差（分别为  $72.9^\circ \pm 5.8^\circ$  和  $88.0^\circ \pm 5.6^\circ$ ；图 2）。西伯利亚和华南相对于华北克拉通的顺时针旋转导致蒙古-鄂霍茨克洋和古特提斯洋的最终闭合。综合东亚各地块古地磁数据，我们重建了东亚各块体早三叠世古地理格局（图 3）。

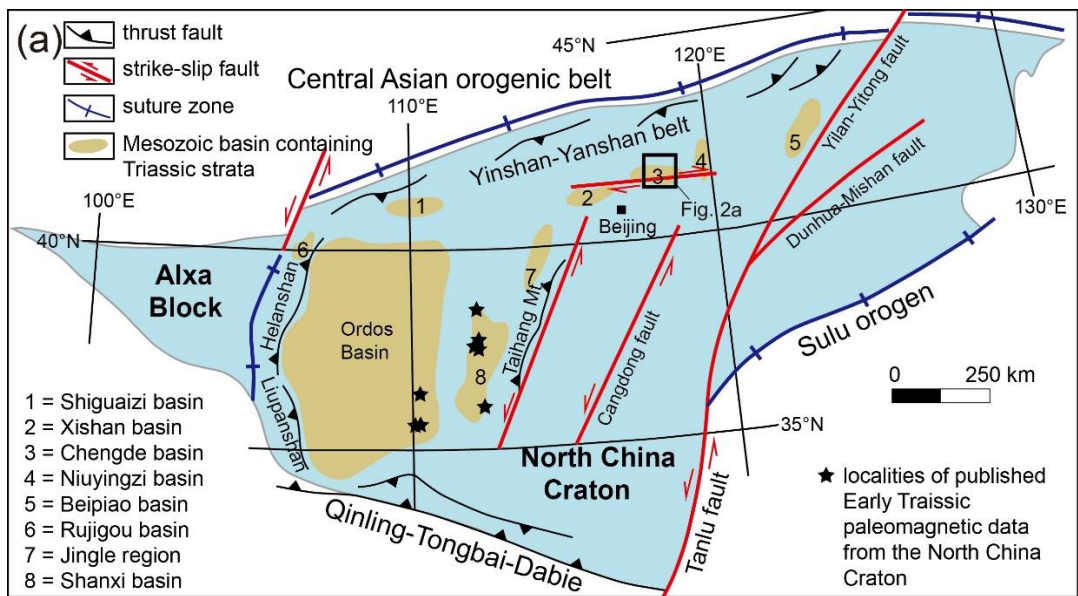


图 1. 华北克拉通构造和中生代沉积盆地分布简图(a)及承德盆地地层分布和采样点(b-d), 星号代表取样点

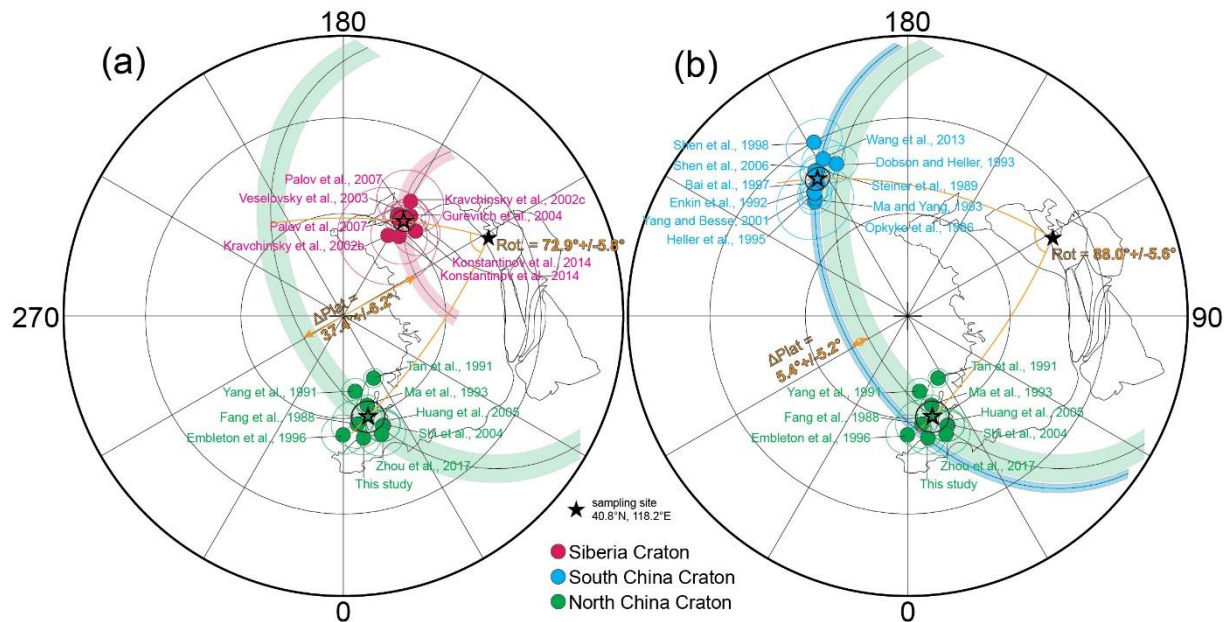


图 2. 华北、华南和西伯利亚克拉通早三叠世古地磁极对比图

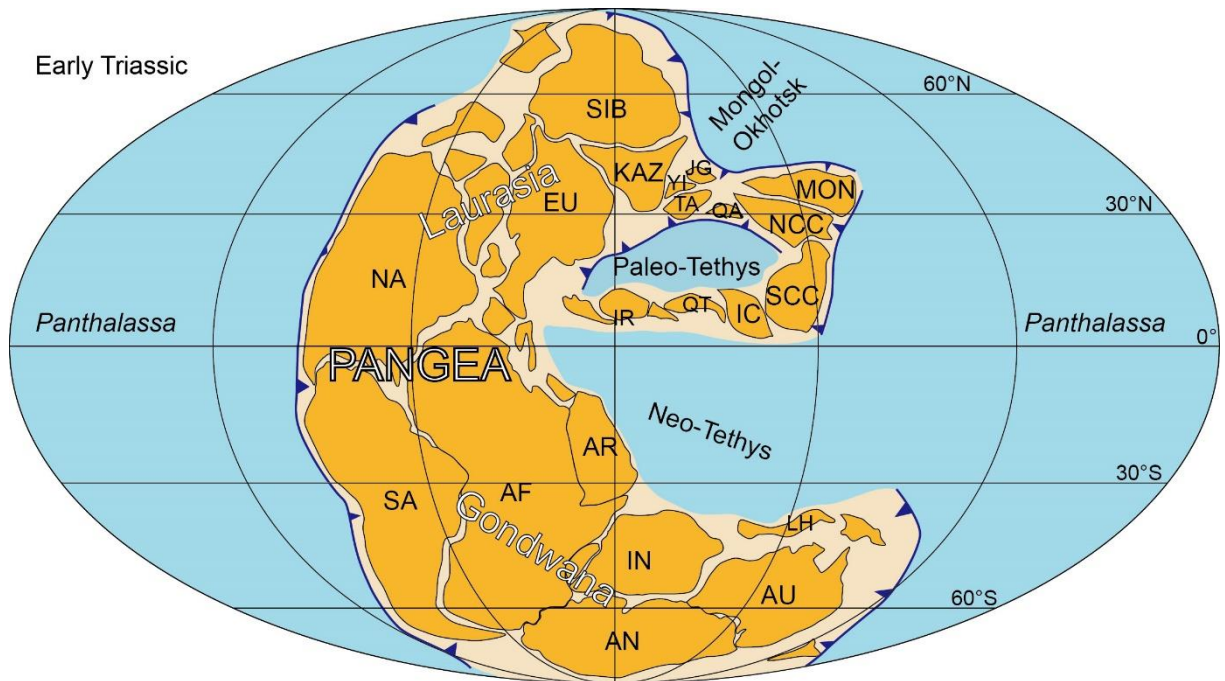


图 3. 早三叠世古地理重建图

成果发表于 *Journal of Geophysical Research: Solid Earth* 上。Zhao, P., Appel, E., & Xu, B. (2020). An inclination shallowing-corrected Early Triassic paleomagnetic pole for the North China Craton: Implication for the Mesozoic geography of Proto-Asia. *Journal of Geophysical Research: Solid Earth*, 125, e2020JB019489. <https://doi.org/10.1029/2020JB019489>。



作者简介：赵盼，中国科学院地质与地球物理研究所副研究员，从事构造古地磁研究。本科毕业于中山大学，在北京大学获得博士学位。2017-2019 在德国图宾根大学做洪堡学者博士后，2019 年回国工作，受中科院百人计划资助。

## ESR: 中布容气候两阶段转型及其对中更新世人类分异演化的环境调控

寒冷的冰期与温暖的间冰期交替变化是第四纪气候的显著特征。冰期时，全球变冷，南北半球高纬度冰盖大幅扩张。间冰期时，全球变暖，两极冰盖消融，万物复苏。当前人类正处于一个异常温暖的超级间冰期时代，过去一万年以来的间冰期气候对人类从温暖的低纬度地区向寒冷的高纬度地区扩散以及人类社会的发展具有重要影响。研究表明我们目前所处的超级间冰期在距今40万年前开始出现，而在这之前的间冰期远没有过去40万年里的间冰期温暖。发生在40万年前的这次间冰期气候转型在古气候学研究中被称为中布容气候转型。

近日，由中国科学院地球环境研究所敖红研究员和安芷生院士、南方科技大学海洋磁学中心刘青松教授、香港大学柳中晖副教授等组成的中国研究团队联合澳大利亚国立大学和英国自然历史博物馆等国际研究团队，提出中布容气候转型具有两阶段演化特征的新假说，并且指出这次气候转型可能对同时期发生的中更新世人类分异演化具有重要的环境调控作用。

研究人员综合80万年以来的全球海陆古气候记录，发现北半球大陆气候在50万年前的间冰期就比之前的间冰期时代要温暖了，虽然南半球间冰期气候在这时并没有显著变暖。这一南北半球气候的不对称变化导致ITCZ北移，北半球主要季风区的降雨增加，并且全球碳库也发生了变化。研究人员把这一间冰期气候转变称为中布容气候转型第一阶段。这一阶段的气候变化对紧随其后的冰期和间冰期气候在全球尺度的转变（即中布容气候转型第二阶段）奠定了基础。中布容气候转型第二阶段主要表现为全球尺度的大气二氧化碳增加，南北半球温度都升高，南北极的冰盖减少，海平面升高。这些变化使得东亚季风区的降雨仍然维持在较高的水平。

研究人员进一步综合古气候记录与考古记录，发现中布容气候转型伴随着人类的分异演化，包括尼安德特人和丹尼索瓦人在欧亚大陆出现，现代人在非洲出现。与此同时，石器打制技术也开始从手斧文化向更加先进的勒瓦娄哇(Levallois)文化转变。这表明这时期人类的进化与中布容气候转型密切相关。

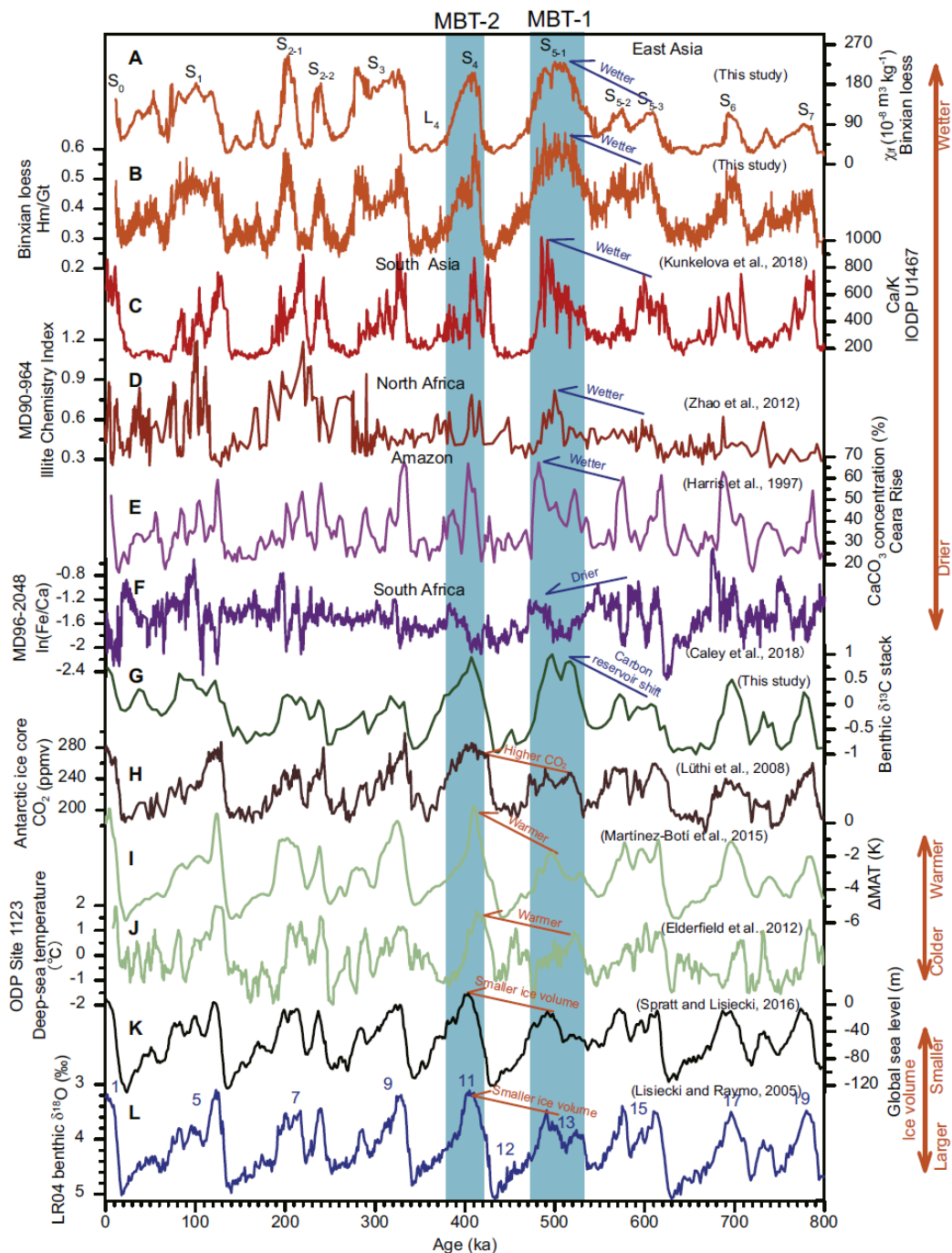


图1 中布容气候转型的两个阶段

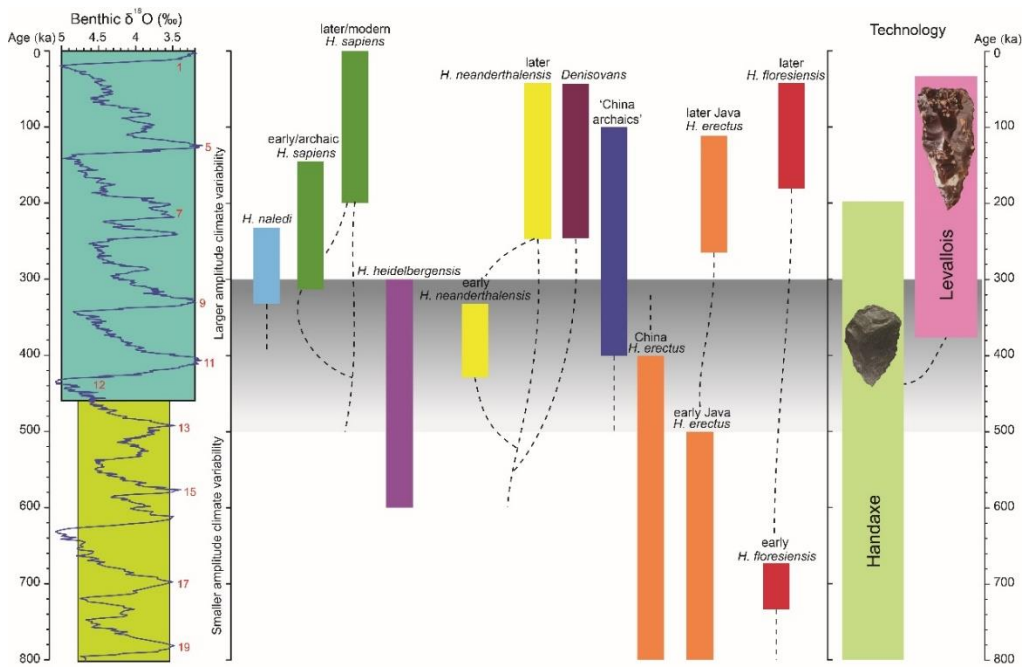


图2 中布容气候转型与中更新世人类分异演化

该研究成果于近期发表在 Earth-Science Reviews (Ao, H., et al., 2020. Two-stage mid-Brunhes climate transition and mid-Pleistocene human diversification. Earth-Science Reviews 210: 103354)。该研究得到第二次青藏科考计划、中国科学院、国家自然科学基金、国家科技部和陕西省科技厅的联合资助。



作者简介：敖红，中国科学院地球环境研究所，主要从事新生代环境磁学、古地磁学、第四纪地质学和古气候学的交叉研究；Eelco J. Rohling，澳大利亚国立大学；Chris Stringer，英国自然历史博物馆；Andrew P. Roberts 澳大利亚国立大学；Mark J. Dekkers，乌得勒支大学；Guillaume Dupont-Nivet，雷恩第一大学；Jimin Yu，澳大利亚国立大学；刘青松，南方科技大学；张鹏，中国科学院地球环境研究所；柳中晖，香港大学；马小林，中国科学院地球环境研究所；周卫健，中国科学院地球环境研究所；金章东，中国科学院地球环境研究所；肖国桥，中国地质大学（武汉）；王宏，北京大学；孙强，西安科技大学；杨萍果，山西师范大学；彭贤哲，中国地质大学（武汉）；石正国，中国科学院地球环境研究所；强小科，中国科学院地球环境研究所；安芷生，中国科学院地球环境研究所。

## 岩石磁学演绎

### 第 33 章 磁学性质的温度效应参数总结

温度对应着热能，扰动磁矩的定向排列，因此对磁性材料的磁学性质有直接的影响。测量磁化率或者饱和磁化强度( $M_s$ ) 随温度变化的曲线时会发现，测量值在超过某一温度后会急剧下降，意味着热能已经完全打乱了磁性材料中自旋的交换相互作用，从而使磁性材料变成了顺磁性。该温度点对于铁磁性材料来说，是居里温度点( $T_C$ )，对于反铁磁性（imperfect antiferromagnets）材料来说，是尼尔温度点( $T_N$ )。这是鉴别磁性矿物非常重要的温度效应，因为化学计量的磁性矿物有着各自特征的  $T_C$  或  $T_N$ 。当  $T < T_C$  时，磁性矿物的性质也存在着明显的变化。较低的温度时，磁各向异性能相对热扰动具有优势，磁矩可以保持沿易磁化方向排列，而不随外场（弱场）方向排列，即可以保存剩磁，处于阻挡状态。随温度升高至某一临界点时，热扰动增强至恰好克服各向异性能对磁矩的束缚，磁矩变得容易响应外场，即容易被磁化，所以磁化率迅速升高，这是矿物的阻挡状态与解阻状态的临界温度点，称为阻挡温度( $T_b$ )或解阻温度( $T_{ub}$ )。 $T > T_b$  后材料变为超顺磁性（SP，其对磁场的响应行为与顺磁性物质相似，可以用相同的方程描述，但是由于自旋的交换作用仍然保留，所以具有很强的磁性，因此称为超顺磁性）。但随着温度的继续升高，由于  $M_s$  的下降， $k$  也会下降。因此在磁化率变温曲线( $k$ - $T$ )上， $T_b$  处会出现一个峰值，即 Hopkinson 峰。 $T_b$  随矿物粒径的增加而增加，趋向于  $T_C$ 。自然样品中，矿物粒径通常具有较宽的分布，在  $k$ - $T$  曲线上对应着较宽的 Hopkinson 峰，而且( $T_b$ )max 接近  $T_C$ 。

化学计量磁铁矿的  $T_C$  为 580 °C，赤铁矿的  $T_N$  为 675 °C [Dunlop and Özdemir, 1997]，但如果矿物不是标准化学计量的（如受到类质同象阳离子替代或晶格缺陷影响）（图 1），这个特征温度会发生变化。比如，在自然环境中，赤铁矿中经常出现铝替代的现象，称为含铝赤铁矿(Al-hematite) [Cornell and Schwertmann, 2003]。铝替代造成了赤铁矿  $T_N$  的下降从而接近磁铁矿的  $T_C$ 。尽管如此，通常含铝赤铁矿的矫顽力仍然大于磁铁矿 [e.g., Roberts et al., 2006; Liu et al., 2007b]。针铁矿的  $T_N$  约为 120 °C，但晶格中铝含量的增加也会造成  $T_N$  下降从而接近室温，同时也会造成针铁矿的矫顽力急剧下降，从正常的 10 ~ 20 T 降

至于磁铁矿相当的水平（几十 mT，甚至更低，*Liu et al.* [2006a]）。磁赤铁矿理论上的  $T_C$  为  $645\text{ }^{\circ}\text{C}$  [*Dunlop and Özdemir*, 1997]，但因该矿物热稳定性差，容易转化为其他磁性矿物（通常为磁铁矿和赤铁矿），其  $T_C$  难以确定，但这个性质对应一个重要应用。中国黄土高原的古土壤样品的典型  $k-T$  上，在  $300$  到  $450\text{ }^{\circ}\text{C}$  之间常见到磁化率的明显下降，这个特征被认为是古土壤中的磁赤铁矿加热发生转化引起的[e.g., *Liu et al.*, 2005b]。钛磁铁矿的  $T_C$  小于磁铁矿，而且与钛含量成反比。利用这一点，通过  $k-T$  可以判断铁离子被替换的程度 [*Akimoto*, 1962; *Nishitani and Kono*, 1983]。单斜磁黄铁矿的  $T_C$  为  $325\text{ }^{\circ}\text{C}$  [*Dekkers*, 1989a]，而胶黄铁矿在  $280\text{ }^{\circ}\text{C}$  以上会发生热转化 [e.g., *Snowball and Thompson*, 1988; *Krs et al.*, 1992; *Roberts*, 1995; *Dekkers et al.*, 2000]，虽然已知  $T_C$  大于  $400\text{ }^{\circ}\text{C}$  [*Chang et al.*, 2008; *Roberts et al.*, 2011a]，但如何取得准确的值仍是个挑战。高温测量的一个弊端是在加热/冷却过程中可能会出现次生磁性矿物，从而影响实验结果。

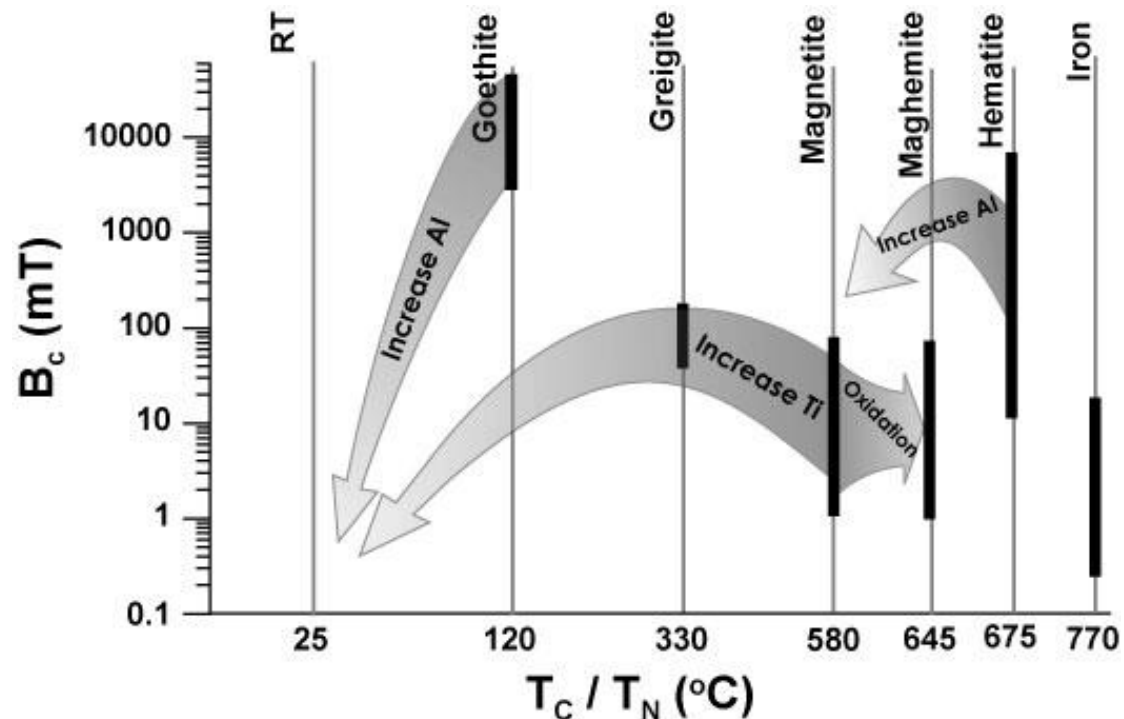


图 1 不同磁性矿物  $B_c$  和  $T_C(T_N)$  之间的相关性。其中，箭头代表同形替代和氧化对这些矿物磁学性质的影响，RT 指示室温。

综上所述，在  $300\text{--}400\text{ }^{\circ}\text{C}$  这个温度段，包括多种矿物的居里点，也容易发

生热转化，钛磁铁矿，磁赤铁矿，胶黄铁矿和磁黄铁矿的出现都会影响这个温度段的热磁测量信号。因此单凭热磁测量手段，很难解释清楚矿物相[e.g., *Roberts and Pillans*, 1993]，必须借助其它手段。铁硫化物与铁氧化物可以很容易利用 SEM 观测加以区分，因为磁黄铁矿和胶黄铁矿具有特殊的微观结构和组成 [e.g., *Roberts et al.*, 2010, 2011a]。一阶反转曲线(first-order reversal curve, FORC)图 [Pike et al., 1999; *Roberts et al.*, 2000] (参见 2.3) 的使用可以给出磁性矿物间的磁相互作用情况，而磁性的铁硫化物由于其特殊的结构通常具有很强的相互作用[e.g., *Rowan and Roberts*, 2006; *Roberts et al.*, 2006]，但也非必然[e.g., *Roberts et al.*, 2011a]。高温测量方法本身的局限性意味着它难以精确地确定样品中的磁性矿物成分，需要借助更多的辅助方法。

低温测量可以为判断磁性矿物成分提供非常有价值的辅助信息，这是因为磁性矿物性质在低温同样存在显著的变化。比如磁铁矿磁矩在晶格中的易磁化方向会在 120 K 附近随晶格形状的变化而发生明显的变化，这个相变就是 Verwey 转换[Verwey, 1939]，相变的温度记为  $T_V$ 。某些赤铁矿也有特征的低温相变，称为 Morin 转换，对应温度  $T_M$  在 250 K 附近[Morin, 1950]。单斜磁黄铁矿在 30-34 K 也有相变[Dekkers et al., 1989a; Rochette et al., 1990]，称为 Besnus 转换[Rochette et al., 2011]。这些低温转换特征是鉴别相应矿物的重要标志，比如低温测量中出现的略低的  $T_V$  (~110 K) [Pan et al., 2005; Li et al., 2009a, b]，结合 FORC 图上无相互作用的 SD 信号，可以作为样品中存在生物成因磁铁矿的判据 [参见 Egli et al., 2010; *Roberts et al.*, 2011b]。如果高温测量中出现~675 °C 的  $T_N$ ，而低温测量又出现 Morin 转换（某些赤铁矿的特征），则赤铁矿的存在是毋庸置疑的。不过低温没有特征转换现象，不代表能够排除某些矿物的存在。例如，胶黄铁矿并没有特征低温转换[e.g., Chang et al., 2009]，不是所有磁铁矿（赤铁矿）都表现出 Verwey 转换（Morin 转换）。针铁矿虽然没有特征的低温转换，但却有特殊的低温行为[e.g., Dekkers, 1989b; Rochette and Fillion, 1989; Liu et al., 2004b, 2006a; Guyodo et al., 2006a]，可以作为其存在的判据。

低温转换的过程受到矿物自身性质的影响。化学计量的磁铁矿的  $T_V$  通常在 ~120-122 K 之间， $T_V$  前后磁化强度的变化幅度则与粒径有关。MD 磁铁矿的 Verwey 转换要比 SD 磁铁矿明显[Dunlop and Özdemir, 1997]。氧化的磁铁矿的相

变过程受到压制,  $T_V$  以及  $T_V$  处磁化强度差都随氧化程度增强而下降, 直至消失 [Özdemir *et al.*, 1993; Cui *et al.*, 1994]。其他导致磁铁矿化学计量关系发生变化的因素 (如同质类象替代) 一般都会造成  $T_V$  的下降以及相变过程趋缓。

当赤铁矿从较高温度冷却经过 Morin 转换点( $T_M$ )时, 其各向异性常数的符号改变, 意味着赤铁矿亚晶格中的自旋方向由沿晶格基面变为晶格对称轴(c 轴)。同磁铁矿一样,  $T_M$  也受到多种因素影响。粒径小于 10-20 nm 的赤铁矿的 Morin 转换完全被抑制 [Bando *et al.*, 1965; Ayyub *et al.*, 1988]。杂质、晶格空位、应变积累以及晶格缺陷都会降低  $T_M$  [Morin, 1950; Morrish, 1994]. 另外, 晶型对  $T_M$  也有重要的影响 [Mitra *et al.*, 2009]。

## 文献速递

### 1. 侏罗纪早期大洋缺氧事件时期碳释放和风化作用直接相关



翻译人：仲义 zhongy@ustech.edu.cn

David B. Kemp, David Selby, and Kentaro Izumi., *Direct coupling between carbon release and weathering during the Toarcian oceanic anoxic event [J], Geology, 2020(48), 976-980.*  
[https://doi.org/10.1130/G47509.1.](https://doi.org/10.1130/G47509.1)

**摘要：**硅酸盐风化作用代表地球气候系统最大反馈机制，在百万年尺度上可以有助于稳定大气 CO<sub>2</sub> 含量和温度变化。而在更短的时间尺度上理解人为 CO<sub>2</sub> 的演化和风化作用的反应性不是很清楚。本文作者利用高精度 Os 同位素揭示了侏罗纪早期缺氧事件时期（T-OAE, 182 Ma）全球化学风化的变化。结果显示，该时期外源碳库的碳同位素明显降低与富集 <sup>12</sup>C 的碳大量释放有关。放射性 Os 同位素向海洋的通量随着碳同位素的降低而增加，表明大量碳排放与全球大陆地壳风化增强作用是同步耦合的。这种碳同位素的突变前人解释为千年尺度甲烷水合物释放和陆源碳的释放有关，这与风化作用的迅速增加也是同步的。在每个突变时期碳的大量注入，全球的风化强度会增加 40%。本文帮助理解和验证了先前在 T-OAE 时期化学风化作用预估，总之，全球风化速率可能在整个事件时期会增加 6 倍。

**ABSTRACT:** Silicate weathering represents a major feedback mechanism in the Earth's climate system, helping to stabilize atmospheric CO<sub>2</sub> levels and temperature on million-year time scales. On shorter time scales of greater relevance to understanding the fate of anthropogenic CO<sub>2</sub>, the efficacy and responsiveness of weathering is less clear. Here, we present high-resolution osmium-isotope data that reflect global chemical weathering from a stratigraphically thick record of the early Toarcian oceanic anoxic event (T-OAE; ca. 182 Ma). A pronounced decrease in the carbon-isotope composition of exogenic carbon reservoirs during this event has been linked to the large-scale release of <sup>12</sup>C-enriched carbon. Our data indicate that the flux of radiogenic osmium to the oceans increased in lockstep with the decrease in carbon-isotope values, demonstrating a geologically synchronous coupling between massive carbon release and enhanced global continental crust weathering. We show that abrupt shifts in carbon isotopes, previously interpreted as millennial-scale methane hydrate melting or terrestrial carbon-release events, are coeval with rapid increases in

weathering. Global weathering may have increased by >40% across each of these intervals of rapid carbon injection. Our results help to reconcile previous estimates of weathering change during the T-OAE, and support the view that, overall, global weathering rates may have increased six-fold through the entire event.

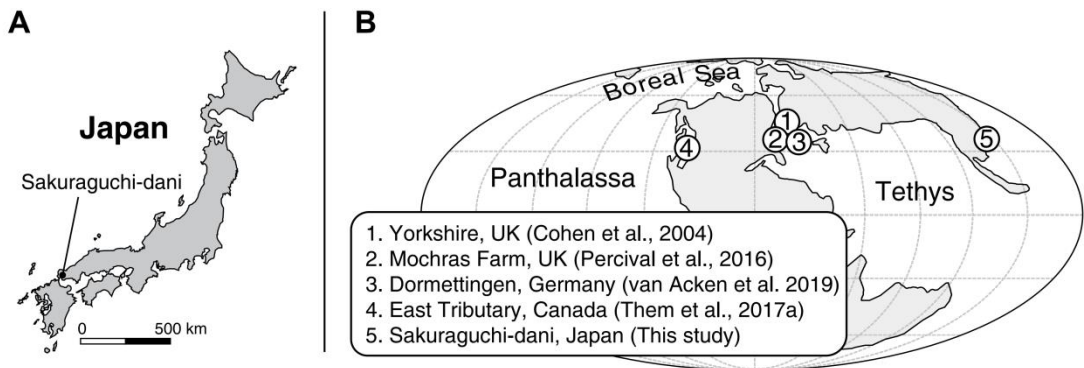


**Figure 1.** Maps showing modern location (A; 34° 08' N, 131° 03' E) and paleogeographic (B; ca. 182 Ma) location of the Sakuraguchi-dani site, Japan, and locations of previous early Toarcian Os-isotope studies (see Fig. 3). East Tributary refers to the East Tributary of Bighorn Creek. Redrawn from Izumi et al. (2012).

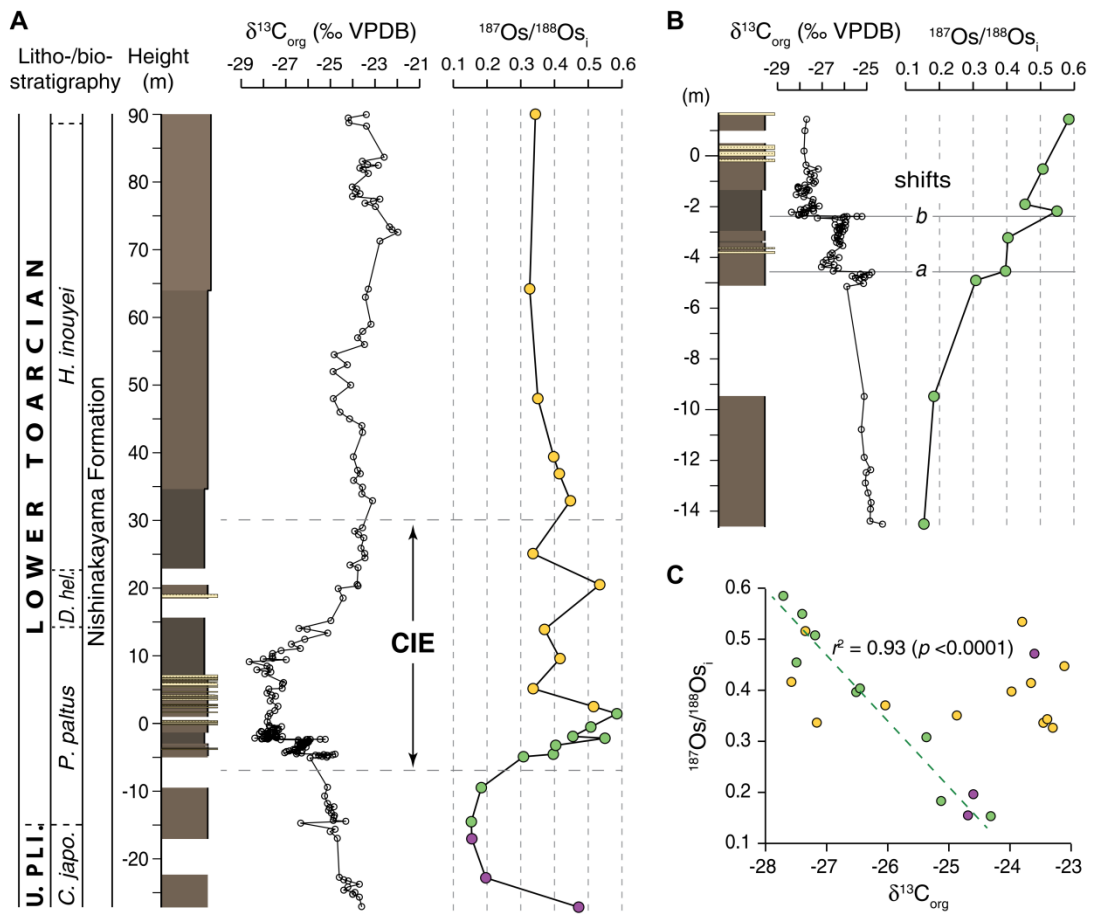


**Figure 2.** Os-isotope and organic  $\delta^{13}\text{C}$  ( $\delta^{13}\text{C}_{\text{org}}$ ) through the Sakuraguchidani succession, Japan. (A) Sedimentary log with  $^{187}\text{Os}/^{188}\text{Os}_i$  (i—initial) and  $\delta^{13}\text{C}_{\text{org}}$  variations against lithostratigraphy and ammonite zones (C.japo.— *Canavaria japonica*; P. paltus — *Paltarpites paltus*; D. hel.— *Dactylioceras helianthoides*; H. inouyei— *Harpoceras inouyei*). Color-coding divides  $^{187}\text{Os}/^{188}\text{Os}_i$  data into pre – carbon-isotope excursion (CIE) data (purple), data primarily through onset of the CIE (minimum to maximum  $^{187}\text{Os}/^{188}\text{Os}_i$ , green), and data above these (orange). Log is from Izumi et al. (2012, 2018a) and field observations.  $\delta^{13}\text{C}_{\text{org}}$  is from Izumi et al. (2012, 2018a, 2018b), Kemp and Izumi (2014), and this study. PLI.—Pliensbachian; VPDB—Vienna PeeDee belemnite. (B) Close-up of the CIE onset, showing abrupt shifts in  $^{187}\text{Os}/^{188}\text{Os}_i$  across  $\delta^{13}\text{C}_{\text{org}}$  shifts a and b. (C) Crossplot of  $^{187}\text{Os}/^{188}\text{Os}_i$  and  $\delta^{13}\text{C}_{\text{org}}$  showing the negative correlation between  $^{187}\text{Os}/^{188}\text{Os}_i$  and  $\delta^{13}\text{C}_{\text{org}}$  across the onset of the CIE/ $^{187}\text{Os}/^{188}\text{Os}_i$  excursion, and no correlation below and above this interval.

## 2. 在 OAE2 期间海洋有机碳埋藏增加森林大火频率



翻译人：蒋晓东 [jiangxd@sustech.edu.cn](mailto:jiangxd@sustech.edu.cn)

Boudinot F G, Sepúlveda J, *Marine organic carbon burial increased forest fire frequency during Oceanic Anoxic Event 2* [J]. *Nature Geoscience*, 2020, 13, 693-698.

<https://doi.org/10.1038/s41561-020-0633-y>

**摘要：**在大洋缺氧事件 2 (OAE2) ~94 Ma, 火山驱动营养物质输入海洋，刺激生产力爆发和有机质埋藏。在这次事件中亏损  $^{13}\text{C}$  有机质的埋藏引起沉积物中  $^{13}\text{C}$  富集，而约 2 % 的  $^{13}\text{C}$  亏损打断了该事件的前半时（以 Plenus 闻名），因此在 OAE2 间碳循环的反馈仍然不太清楚。本研究基于美国西部内海道沉积物的分析，提供了有机地球化学证据（例如高热形成的多环芳烃），结果表明 Plenus 期间森林大火频率增加。决定 OAE2 间大气二氧化碳含量与碳同位素以及生物量的碳质量平衡方程，使美国西部大火增强而成为广泛增加的森林大火的原因，该大火能够单独引起 2 %  $^{13}\text{C}$  亏损。植物生物标志物表明当地的沉积和植物种类并未发生显著变化，表明因广泛有机碳埋藏而上升的大气二氧化碳浓度增加了湿润森林系统发生大火的频率。植物生物标志物同时表明森林大火扩大了陆地有机碳和营养物质到海洋的通量，这可能增强了海洋生产力、有机碳埋藏，并且在 Plenus 末期时使富  $^{13}\text{C}$  沉积物恢复到原来水平。这反馈的程度已经影响了 Plenus 期间全球的生物地球化学循环和 OAE2，以及地球历史的其他事件，因而还需进一步研究。

**ABSTRACT:** Volcanic-driven nutrient flux to the oceans stimulated marine productivity and organic matter burial during Oceanic Anoxic Event 2 (OAE2; ~94 million years ago). While the preferential burial of  $^{13}\text{C}$ -depleted organic matter led to a general  $^{13}\text{C}$  enrichment of sediments during the event, a 2%  $^{13}\text{C}$  depletion punctuated the first half of the event (known as the Plenus), raising questions about carbon cycle feedbacks during OAE2. Here we present organic geochemical evidence (for example, pyrogenic polycyclic aromatic hydrocarbons) from the Western Interior Seaway that indicates increased forest fire frequency in the western United States during the Plenus. Carbon mass balance equations, which account for the amount and carbon isotopic composition of atmospheric  $\text{CO}_2$  and forest biomass during OAE2, potentiate fires in the western United States as

part of a widespread increase in forest fires that could have alone caused the global 2‰  $^{13}\text{C}$  depletion during the Plenus. Plant biomarkers suggest that local precipitation and plant type did not change significantly, indicating that elevated atmospheric oxygen levels from widespread organic carbon burial increased the frequency of fires in wet forest ecosystems that were extensive during OAE2. Plant biomarkers also indicate that forest fires amplified the flux of terrestrial organic matter and nutrients to the oceans, which may have enhanced marine productivity, organic carbon burial and the return to  $^{13}\text{C}$ -enriched sediments at the end of the Plenus. The extent that this feedback impacted global biogeochemistry during the Plenus and the rest of OAE2, as well as other events in Earth history, warrants further investigation.



**Figure 1.** Palaeogeography of the study area. Palaeomap of the WIS during the earliest Turonian (93.2 Ma; Colorado Plateau Geosystems; ref. 70) indicates water depth (blue shading), main topography and wind direction (arrow, based on isopach maps and discussion in ref. 31). Inset map (location shown in red box on WIS palaeomap) shows SH#1 core (and corresponding Kaiparowits Plateau Section (KPS) outcrops<sup>5,70</sup>) location on modern geography (modified from ref. 5).

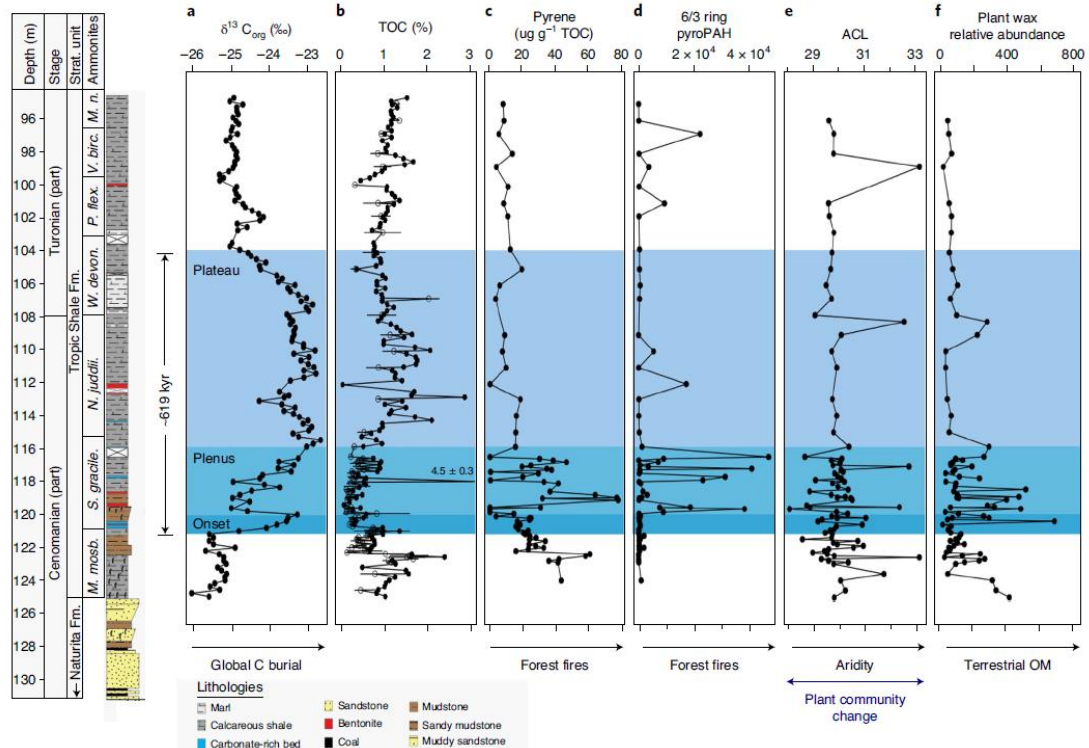


**Figure 2.** Bulk organic carbon and biomarkers from the SH#1 core. Lithology, biostratigraphy and timescale from the Triopic Shale Formation (Fm.) through the upper Cenomanian and lower Turonian (part) are from ref. 5. a, Stable carbon isotopic composition ( $\delta^{13}\text{C}$ ) of bulk organic carbon<sup>5</sup>, with enriched values (to the right) caused by widespread marine organic carbon burial. b, Total organic carbon (TOC (%); closed circles and error bars from ref. 5 and open circles and error bars from ref. 70). c, Pyrene concentration, with higher values indicative of higher forest fire frequency, d, Ratio of six-ring pyroPAHs over three-ring pyroPAHs, with higher values indicating pyroPAH input from forest fires, e, ACL, with higher values derived from increased aridity and/or changes in plant community, and lower values derived from decreased aridity and/or changes in plant community, f, Plant wax relative abundance (n-C<sub>27,29,31,33,35</sub>/n-C<sub>17,19,21,27,29,31,33,35</sub> (ref. 70)), which indicates changes in the input of terrestrial OM to the study area. Dark, medium and light blue indicate the OAE2 onset (121.196–120 mcd), Plenus (120–115.88 mcd) and plateau (115.88–103.93 mcd) phases, respectively. Ammonite genus and species abbreviations: *M. mosb.*, *Metoicoceras mosbyense*; *S. gracile*, *Sciponoceras gracile*; *N. juddii*, *Neocardioceras juddii*; *W. devon.*, *Watinoceras devonense*; *P. flex.*, *Pseudaspidoceras flexuosum*; *V. birc.*, *Vascoceras birchbyi*; *M. n.*, *Mammites nodosoides*.

### 3. 地幔过渡带内滞留的板片前缘控制着东北亚地区新生代陆内高镁安山岩的形成



翻译人：冯婉仪 [fengwy@sustech.edu.cn](mailto:fengwy@sustech.edu.cn)

Xu WL, Chen JH, Wang AH, et al. *Stagnant slab front within the mantle transition zone controls the formation of Cenozoic intracontinental high-Mg andesites in northeast Asia* [J]. *Geology*, 2020, 48. <https://doi.org/10.1130/G47917.1>

**摘要：**东北亚地区新生代陆内高镁安山岩（HMAS）的地球化学和区域地球物理资料为探讨陆内HMAS的形成与太平洋板块俯冲的成因关系提供了契机。与岛弧中的原始HMAS相比，东北亚地区新生代陆内HMAS具有更低的Mg# [ $100 \times \text{Mg}/(\text{Mg} + \text{Fe}^{2+})$ ]值（53–56）和CaO含量（5.8–6.6 wt%）、更高的碱（ $\text{Na}_2\text{O} + \text{K}_2\text{O}$ ）含量（5.15–6.45 wt%），以及更富集的Sr-Nd-Hf同位素组成（ ${}^{87}\text{Sr}/{}^{86}\text{Sr} = 0.7056\text{--}0.7059$ ;  $\varepsilon_{\text{Nd}} = -4.9$ 至 $-3.4$ ;  $\varepsilon_{\text{Hf}} = -4.7$ 至 $-2.6$ ）和更低的Pb同位素比值（ ${}^{206}\text{Pb}/{}^{204}\text{Pb} = 16.76\text{--}19.19$ ;  ${}^{207}\text{Pb}/{}^{204}\text{Pb} = 15.42\text{--}15.45$ ;  ${}^{208}\text{Pb}/{}^{204}\text{Pb} = 36.71\text{--}37.11$ ）。新生代陆内HMAS的Sr-Nd-Pb-Hf同位素组成与东北新生代钾质玄武岩相似，但其 $\text{SiO}_2$ 和 $\text{Al}_2\text{O}_3$ 含量较高，而 $\text{K}_2\text{O}$ 、 $\text{MgO}$ 和轻稀土元素含量较低。这些特征表明新生代陆内HMAS起源于地幔，并且该地幔中循环的古老沉积物和水导致橄榄岩的部分熔融。结合在这些陆内HMAS附近的地幔过渡带（MTZ）存在一个大的低阻异常以及它们出现在东北亚地区MTZ（在600km深度）中滞留板片前缘之上，我们认为滞留板片前缘以及高含量的循环古老沉积物和水控制了东北亚地区新生代陆内HMAS的形成。

**ABSTRACT:** The geochemistry of Cenozoic intracontinental high-Mg andesites (HMAS) in northeast Asia, together with regional geophysical data, offers an opportunity to explore the genetic relationship between the formation of intracontinental HMAS and subduction of the Pacific plate. Compared with primary HMAS in arcs, Cenozoic intracontinental HMAS in northeast Asia have lower Mg# [ $100 \times \text{Mg}/(\text{Mg} + \text{Fe}^{2+})$ ] values (53–56) and CaO contents (5.8–6.6 wt%), higher alkali ( $\text{Na}_2\text{O} + \text{K}_2\text{O}$ ) contents (5.15–6.45 wt%), and enriched Sr-Nd-Hf isotopic compositions ( ${}^{87}\text{Sr}/{}^{86}\text{Sr} = 0.7056\text{--}0.7059$ ;  $\varepsilon_{\text{Nd}} = -4.9$  to  $-3.4$ ;  $\varepsilon_{\text{Hf}} = -4.7$  to  $-2.6$ ) as well as lower Pb isotope ratios ( ${}^{206}\text{Pb}/{}^{204}\text{Pb} = 16.76\text{--}19.19$ ;  ${}^{207}\text{Pb}/{}^{204}\text{Pb} = 15.42\text{--}15.45$ ;  ${}^{208}\text{Pb}/{}^{204}\text{Pb} = 36.71\text{--}37.11$ ). These Cenozoic intracontinental HMAS are similar to Cenozoic potassic basalts in northeast China with respect to their Sr-Nd-Pb-Hf isotopic compositions but have higher  $\text{SiO}_2$  and  $\text{Al}_2\text{O}_3$  contents and lower  $\text{K}_2\text{O}$ ,

MgO, and light rare earth element contents. These features indicate that these Cenozoic intracontinental HMAs originated from the mantle, where recycled ancient sediments and water contributed to partial melting of peridotite. Combined with the presence of a large low-resistivity anomaly derived from the mantle transition zone (MTZ) near these intracontinental HMAs, and their occurrence above the stagnant slab front within the MTZ (at 600 km depth) in northeast Asia, we conclude that the stagnant slab front, with high contents of recycled ancient sediments and water, has controlled the formation of Cenozoic intracontinental HMAs in northeast Asia.

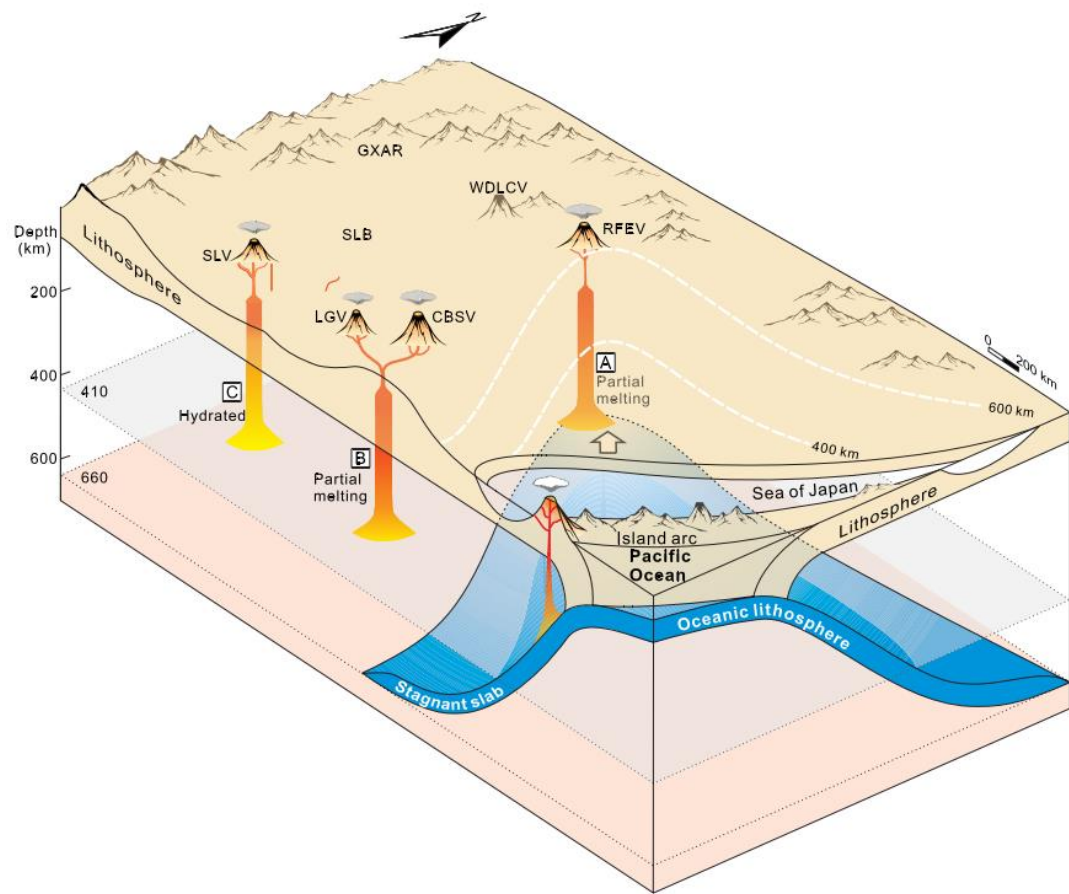


**Figure 1.** Schematic geodynamic model for formation of Cenozoic intracontinental high-Mg andesites in northeast Asia. CBSV—Changbaishan volcano; GXAR—Great Xing'an Range; LGV—Longgang volcano; RFEV—Russian Far East volcano; SLB—Songliao basin; SLV—Shuangliao volcano; WDLCV—Wudalianchi volcano. Surfaces at 410 km and 660 km represent the upper and lower boundaries of the mantle transition zone.

#### 4. 揭示 Powell 海盆的构造域和异常的磁异常特征



翻译人:李园洁 liyj3@sustech.edu.cn

*Catalán M., Martos Y. M., Galindo-Zaldívar J. et al., Unveiling Powell Basin's Tectonic Domains and Understanding Its Abnormal Magnetic Anomaly Signature. Is Heat the Key? [J]. Frontiers in Earth Science, 2020(8). <https://doi.org/10.3389/feart.2020.580675>*

**摘要:** 由大陆岩石圈的裂解产生洋盆是个非常复杂的过程, 受不同因素的影响如深部岩石圈的流变和热结构, 和深部软流圈的动力学。所有过程海洋域的影响, 在小洋盆更容易识别。Powell 洋盆是个小的洋盆, 北边界是南 Scotia 脊, 东边是南 Orkney 微陆块, 西边是南极洲半岛。它形成于渐新世和中新世期间, 但是年龄没有很好的约束, 部分是因为扩张磁异常具有小的幅值。利用这个洋盆可以分析不同裂解和扩张相。为识别 Powell 盆地从裂解开始到停止扩张的不同边界, 作者综合不同数据, 包括重力数据, 磁数据, 多测道地震剖面和测深数据。地震和测深数据用来估计总的构造沉降, 来描述早期裂解到洋壳形成的不同构造域。这个结果结合磁异常数据圈定洋域范围。最后作者分析斯科舍海软流圈分支的侵入在洋盆中磁异常特征的演化中的作用。

**ABSTRACT:** Rifting of continental lithosphere leading to oceanic basins is a complex process conditioned by different factors such as the rheology and thermal structure of the underlying lithosphere, as well as underlying asthenospheric dynamics. All these processes, which finally lead to oceanic domains, can better be recognized in small oceanic basins. Powell Basin is a small oceanic basin bounded to the north by the South Scotia Ridge, to the east by the South Orkney Microcontinent, and to the west by the Antarctic Peninsula. It was formed between the Oligocene and Miocene, however, its age is not well defined, among other reasons due to the small amplitude of its spreading magnetic anomalies. This basin is an ideal framework to analyze the different rifting and spreading phases, which leads from continental crust to the formation of an oceanic domain through different extensional regimes. To identify the different boundaries during the formation of Powell Basin from the beginning of the rifting until the end of the spreading, we use different data sources: magnetic, gravity, multichannel seismic profiles and bathymetry data. We use seismic and bathymetry data to estimate the Total Tectonic Subsidence. Total Tectonic Subsidence has proven to be useful to delineate the different tectonic regimes present from early rifting to the formation of

oceanic seafloor. This result together with magnetic data has been used to delimit the oceanic domain and compare with previous authors' proposals. This method could be applied in any other basin or margin to help delimiting its boundaries. Finally, we analyze the role that an asthenospheric branch intruding from the Scotia Sea played in the evolution of the magnetic anomaly signature on an oceanic basin.

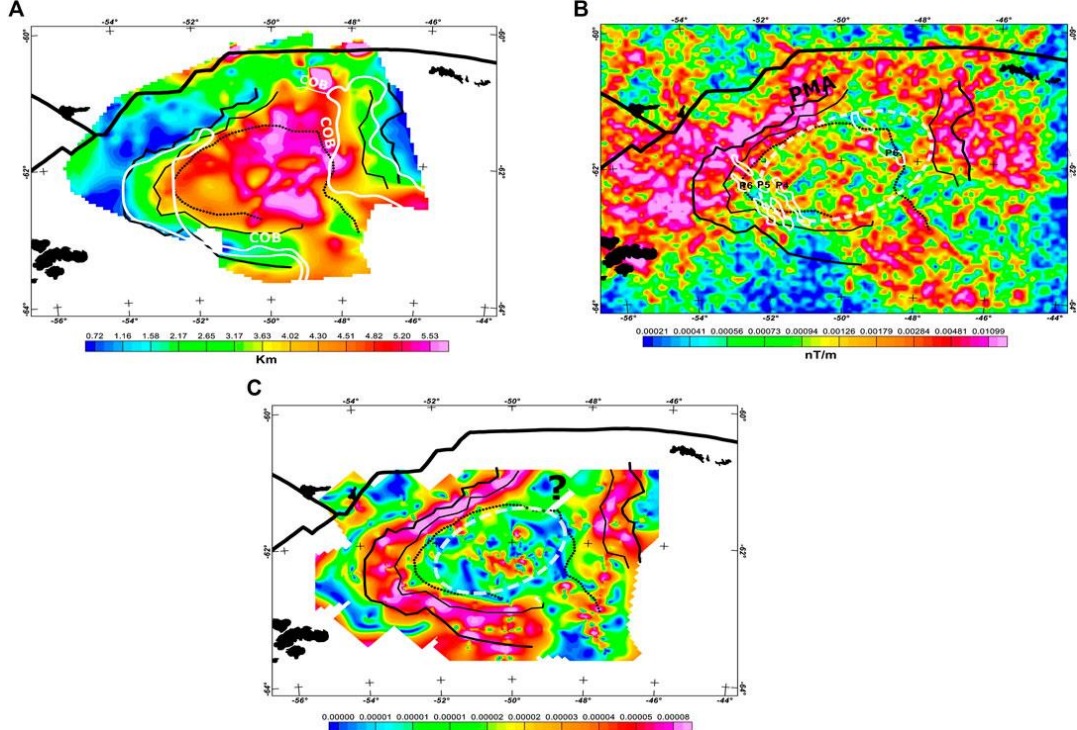


**Figure 1.** A) TTS map. In white King et al. (1997)' s interpretation of several features as follows: A white solid curvilinear polygon in the East and West margins of Powell Basin depicts the location of areas interpreted as extended continental crust. The outer flanks of the previous cited curvilinear polygon was identified as continent-ocean boundary (COB labels in white mark its location). In thin white dotted line COB' s interpreted location (northeastern part of the basin). (B) Analytical signal of the filtered magnetic map. An elliptical white dotted outline marks Powell Basin' s location. In white solid lines some magnetic lineations (P4, P5 and P6) identified in Eagles and Livermore (2002). PMA, Pacific Margin Magnetic Anomaly. (C) TTS horizontal gradient map. Thick and thin black lines delimit abrupt changes on the horizontal gradient magnitude. A black dotted line delimits the outer boundary of the oceanic domain. Plate boundaries in black solid thick lines. A black question mark denotes an area whose continental nature is not concluded.

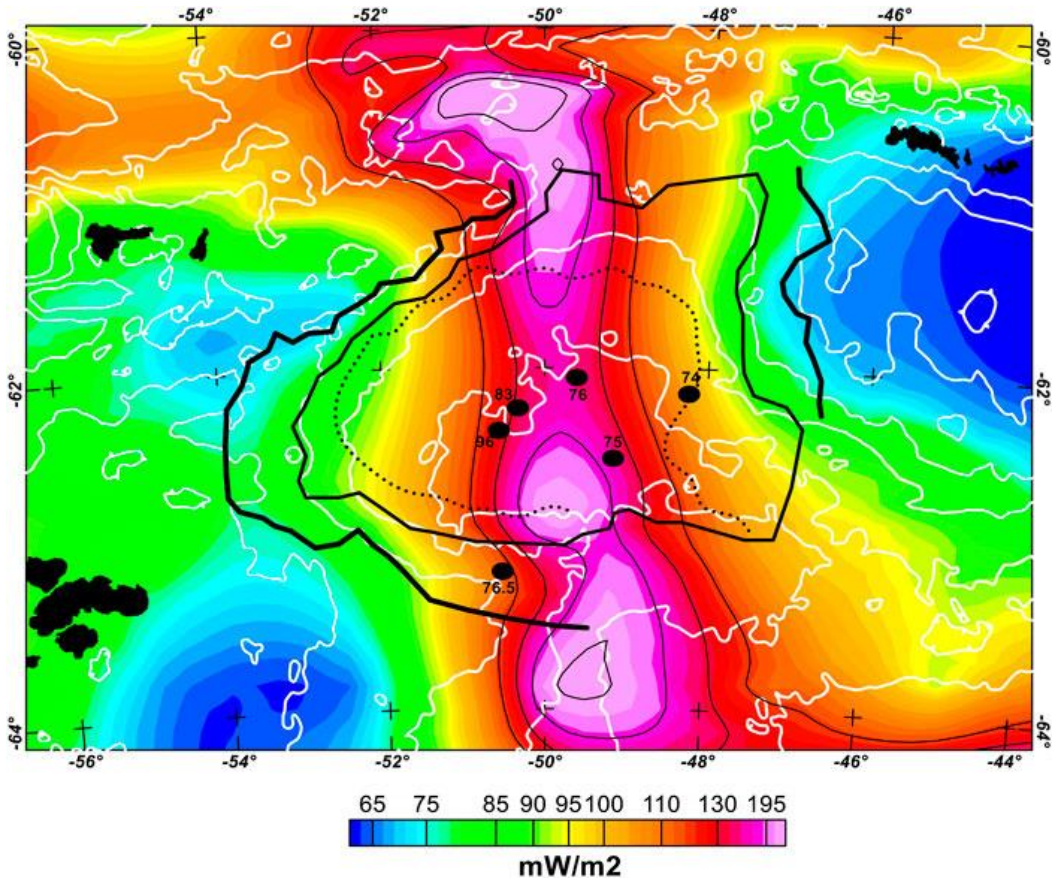


**Figure 2.** HF map derived from magnetic data (see Martos et al., 2019 for details). Thin black contour lines denote HF isolines: 120, 130, and 140 mW/m<sup>2</sup>. Bouguer gravity anomaly contour lines in thick white color. Heat flow values published by Lawver et al. (1994) in mW/m<sup>2</sup>.

## 5. 超越二阶磁各向异性的张量：辉石中定向磁铁矿析出导致的更高阶分量及其对古磁和构造解释的意义

翻译人：柳加波 liujiabo7@gmail.com



Biedermann A R, Jackson M, Chadima M, et al. *Beyond the second-order magnetic anisotropy tensor: higher-order components due to oriented magnetite exsolutions in pyroxenes, and implications for palaeomagnetic and structural interpretations*[J]. *Geophysical journal international*, 2020, 223(2): 915-933. <https://doi.org/10.1093/gji/ggaa355>

**摘要：**硅酸盐矿物中出溶的氧化铁几乎是理想的古地磁记录载体，这是因为它们具有单畴性质，并且受硅酸盐主体保护而避免发生化学变化。因为它们的几何形状受主体硅酸盐晶体特征控制，所以这些出溶物具有形状偏好的取向，该取向最终由硅酸盐的矿物组构决定。从而导致具有可能显著具有各向异性的获得剩磁，这需要校正才能在古方向和古强度研究中做出准确的解释。本文，我们基于转矩测量和旋转磁滞数据，研究了辉石单晶以及含辉石的岩石中磁铁矿出溶物所记录的磁各向异性。图像分析用于表征氧化物的方向分布，从中可以模拟观察到的各向异性。高场转矩信号和相应的模型都包含较高阶的分量，而这些分量不能被通常用于描述磁组构的二阶张量准确地描述。相反，低场各向异性数据没有显示这种复杂性，可以用二阶张量充分描述。因此，硅酸盐基质出溶物的磁各向异性与磁场有关，在解释孤立的磁组构以及进行各向异性校正时应考虑到这一点。

**ABSTRACT:** Exsolved iron oxides in silicate minerals can be nearly ideal palaeomagnetic recorders, due to their single-domain-like behaviour and the protection from chemical alteration by their surrounding silicate host. Because their geometry is crystallographically controlled by the host silicate, these exsolutions possess a shape preferred orientation that is ultimately controlled by the mineral fabric of the silicates. This leads to potentially significant anisotropic acquisition of remanence, which necessitates correction to make accurate interpretations in palaeodirectional and palaeointensity studies. Here, we investigate the magnetic shape anisotropy carried by magnetite exsolutions in pyroxene single crystals, and in pyroxene-bearing rocks based on torque measurements and rotational hysteresis data. Image analysis is used to characterize the orientation distribution of oxides, from which the observed anisotropy can be modelled. Both the high-field torque signal and corresponding models contain components of higher order, which cannot be

accurately described by second-order tensors usually used to describe magnetic fabrics. Conversely, low-field anisotropy data do not show this complexity and can be adequately described with second-order tensors. Hence, magnetic anisotropy of silicate-hosted exsolutions is field-dependent and this should be taken into account when interpreting isolated ferromagnetic fabrics, and in anisotropy corrections.

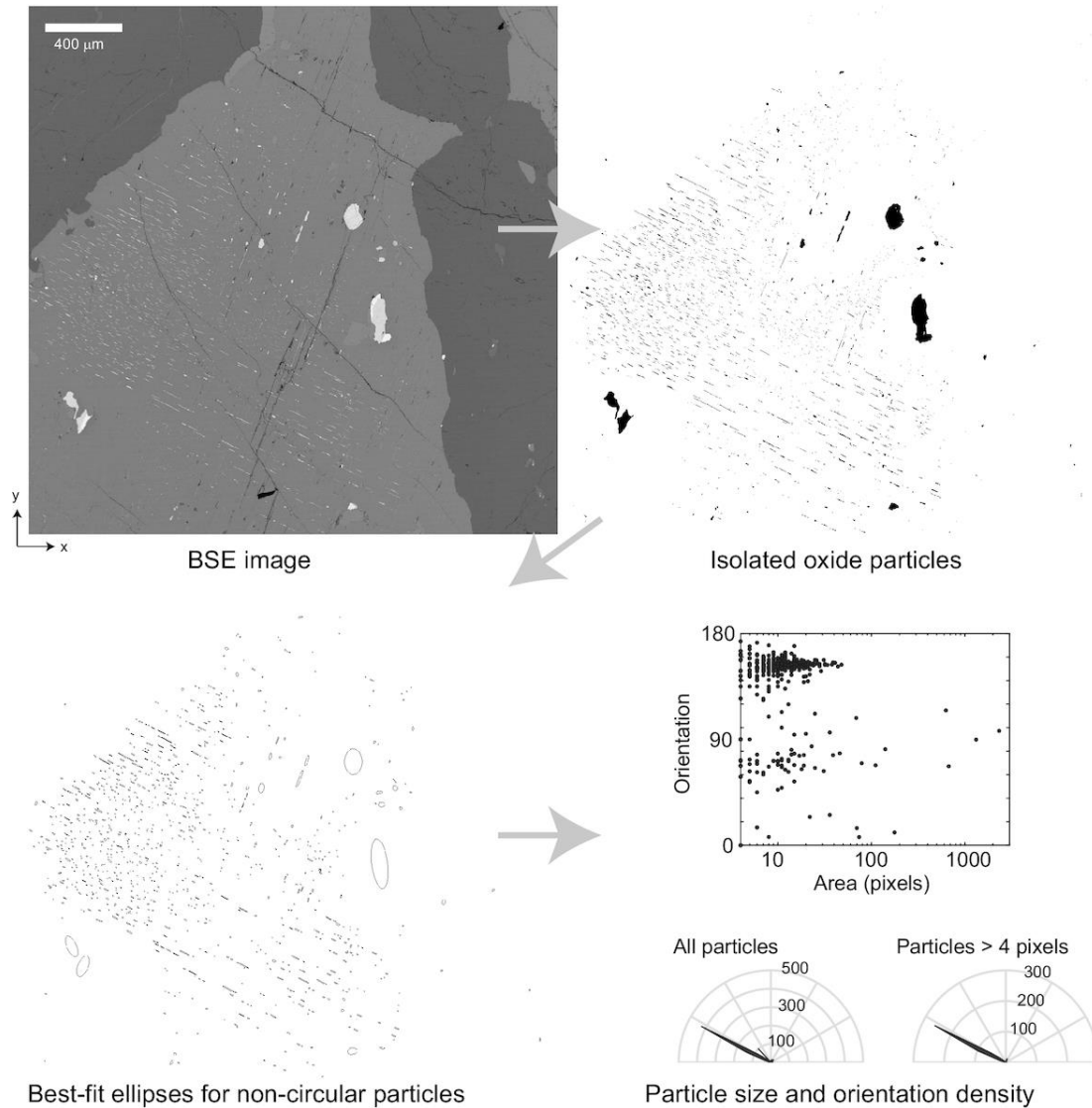


**Figure 1.** Example of the process from BSE image to isolated oxides, best-fit ellipses, and particle size and orientation density distributions. The BSE image shown here pictures part of a clinopyroxene grain in sample NLMD\_NxG\_01010401, with many small exsolved grains of similar orientation, and some larger grains of a different orientation. Numbers in the polar histograms indicate the number of particles of a certain orientation, using  $5^\circ$  bins. Resolution 0.4 pixels per micrometer.

## 6. 河流流量变化与气候和河流扇形成之间的关系



翻译人：刘伟 inewway@163.com

Hansford M R, Plink-Björklund P. **River discharge variability as the link between climate and fluvial fan formation**[J]. *Geology*, 2020, 48(10): 952-956.

<https://doi.org/10.1130/G47471.1>

**摘要：**对于河流扇是否需要特定的气候条件才能形成，有两种截然相反的假设。从地貌和沉积记录中推断气候和构造信号是地质学和地貌学的一个重要目标。因此，获得沉积记录中特别是河流扇中的具体气候变化信号的确认标准是非常有意义的，因为河流扇构成大陆河流记录的相当一大部分。把河流扇形成与气候联系起来的假说明确指出，降水变异性是一个关键的控制因素，因为降水变异性促进了河流扇形成的关键过程——水流变异性、河道不稳定和崩塌。在这里，我们通过对全球分布的 68 条形成扇的河流的流量模式进行定量分析，验证了这一假设。使用一组无量纲度量，我们表明在该数据集中 75% 的形成扇的河流具有高流量变异性。我们进一步分析了下扇流量变化，并讨论了不同水文气候下流量变化的性质，作为一个内部和年际降水波动的函数。我们还研究了具有中低流量变异性的形成扇的河流，得出的结论是，尽管河流流量变异性强烈地促进了河流扇的形成，但如果出现其他有利条件，则具有中低流量变异性的河流也可能形成河流扇。

**ABSTRACT:** There are two contrasting hypotheses on whether fluvial fans need specific climate conditions to form. Deduction of climatic and tectonic signals from landscapes and the sedimentary record is a key aim in geology and geomorphology. It is thus of great interest to obtain recognition criteria for specific climate changes in the sedimentary record in general, and fluvial fans in particular, because they may form the bulk of the continental fluvial record. The hypothesis that links fluvial fan occurrence to climate specifically indicates precipitation variability as a key control, because it promotes streamflow variability, channel instability, and avulsions, which are the key processes involved in fluvial fan formation. Here, we tested this hypothesis by quantitative analyses of discharge patterns from 68 fan-forming rivers that have a global distribution. Using an ensemble of dimensionless metrics, we show that 75% of the fan-forming rivers in this data set have a high discharge variability. We further analyzed down-fan changes in discharge variability and discuss the nature of discharge variability in different hydroclimates as a function of intra- and interannual

precipitation fluctuations. We also examined the fan-forming rivers with moderate to low discharge variability and concluded that although river discharge variability strongly promotes fluvial fan formation, fluvial fans may also be formed by rivers with a moderate or low discharge variability if other favorable conditions that promote avulsions occur.

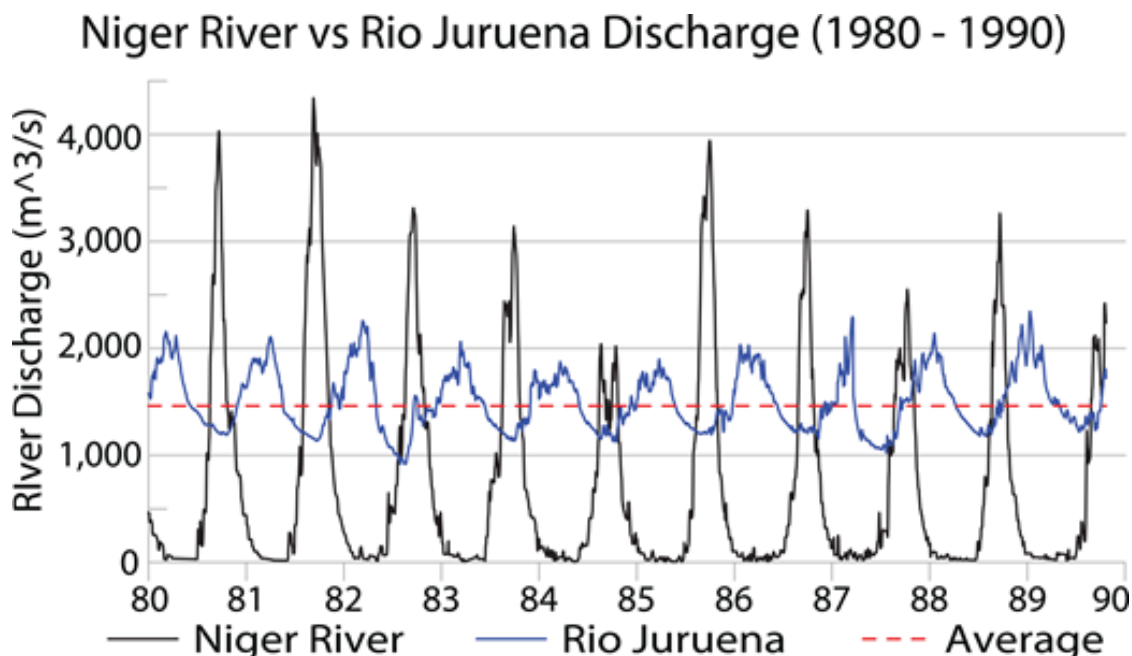


**Figure 1.** Streamflow hydrographs illustrating low (Rio Juruena, DVIa = 0.49; DVIa—discharge variability index) versus high (Rio Niger, DVIa = 3.33) discharge variability for two rivers with similar mean annual discharge (red line).

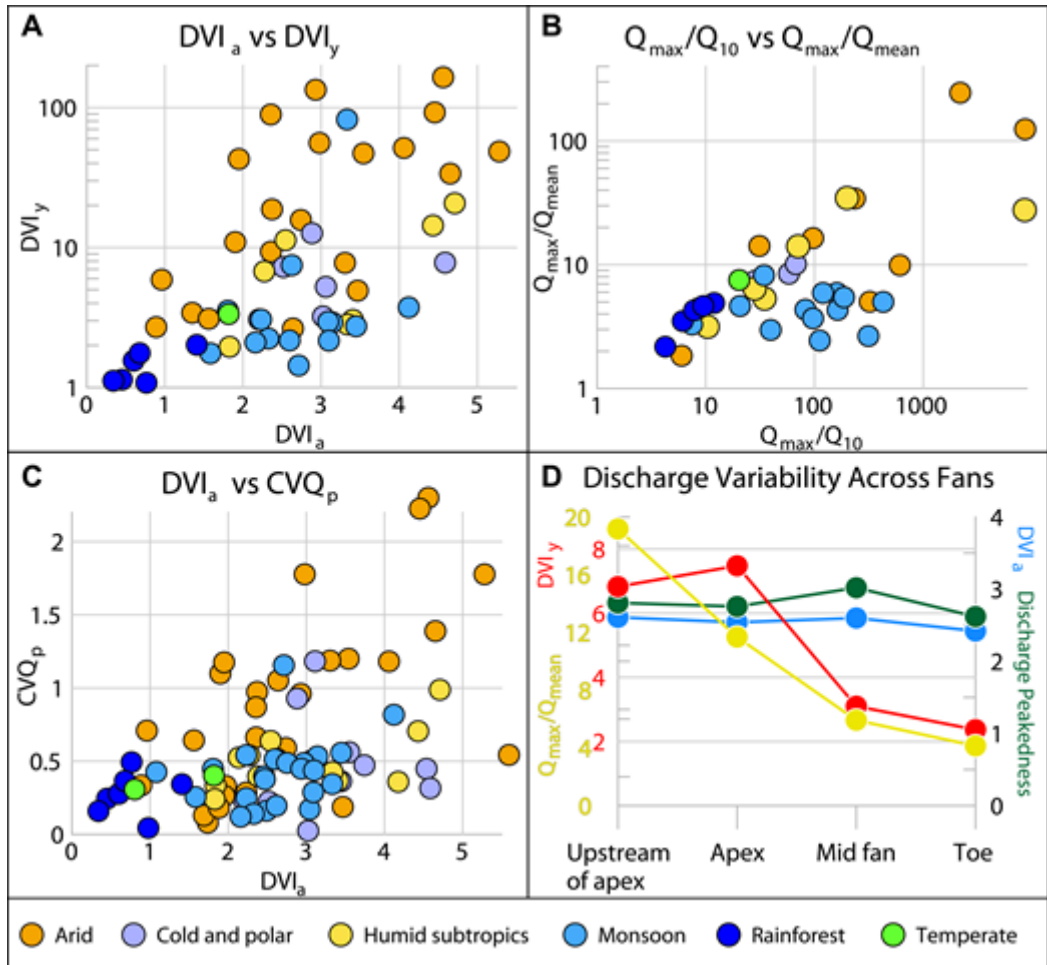


**Figure 2.** Discharge variability in fan-forming rivers, expressed by dimensionless metrics: (A) DVI<sub>a</sub> versus DVI<sub>y</sub>, (B) Q<sub>max</sub>/Q<sub>10</sub> versus Q<sub>max</sub>/Q<sub>mean</sub>, (C) DVI<sub>a</sub> versus CVQ<sub>p</sub>, and (D) downstream discharge variability changes from apex to toe measured by DVI<sub>a</sub>, DVI<sub>y</sub>, Q<sub>max</sub>/Q<sub>mean</sub>, and Qpeak.

## 7. 东非裂谷系统运动学的重新定义



翻译人：曹伟 11930854@QQ.com

*Stamps D.S., Kreemer C., Fernandes R., et al., Redefining East African Rift System kinematics.*

[J]. *Geology*, 2020(49).<https://doi.org/10.1130/G47985.1>

**摘要：**在全球板块运动模型中，东非裂谷系统的板块几何结构和地表运动是最不受约束的。本研究中，我们使用 GPS 数据来约束索马里板块的旋转，并提出该地区新的板块几何结构。此外，我们分析了来自西南印度洋脊的地质数据和马达加斯加的最新 GPS 数据，以确定 Lwandle 微板块的精确运动。研究发现了一个大的变形带，从 Rovuma 微板块的东部边界延伸到科摩罗群岛，包括马达加斯加中部和北部的部分地区。马达加斯加正在裂解，其南部与 Lwandle 微板块一起旋转，同时东部和中南部与索马里板块一起移动。跨越东非裂谷系统的努比亚-索马里板块体系的发散，包括沿着束缚刚性块体的狭窄裂谷段的扩散变形和应变调节。

**ABSTRACT:** East African Rift System plate geometries and surface motions are some of the least constrained in the context of global plate motion models. In this study, we used GPS data to constrain Somalian plate rotation and to suggest a new tectonic plate geometry for the region. In addition, we tested geologic data from the Southwest Indian Ridge and new GPS data on Madagascar to determine refined kinematics of the Lwandle microplate. A zone of broad deformation was discovered, extending from the eastern boundary of the Rovuma microplate, across the Comoros Islands, and including parts of central and northern Madagascar. Madagascar is fragmenting, with southern Madagascar rotating with the Lwandle microplate and a piece of eastern and south-central Madagascar moving with the Somalian plate. Divergence of the Nubian-Somalian plate system across the East African Rift System involves both diffuse deformation and strain accommodation along narrow rift segments that bound rigid blocks.

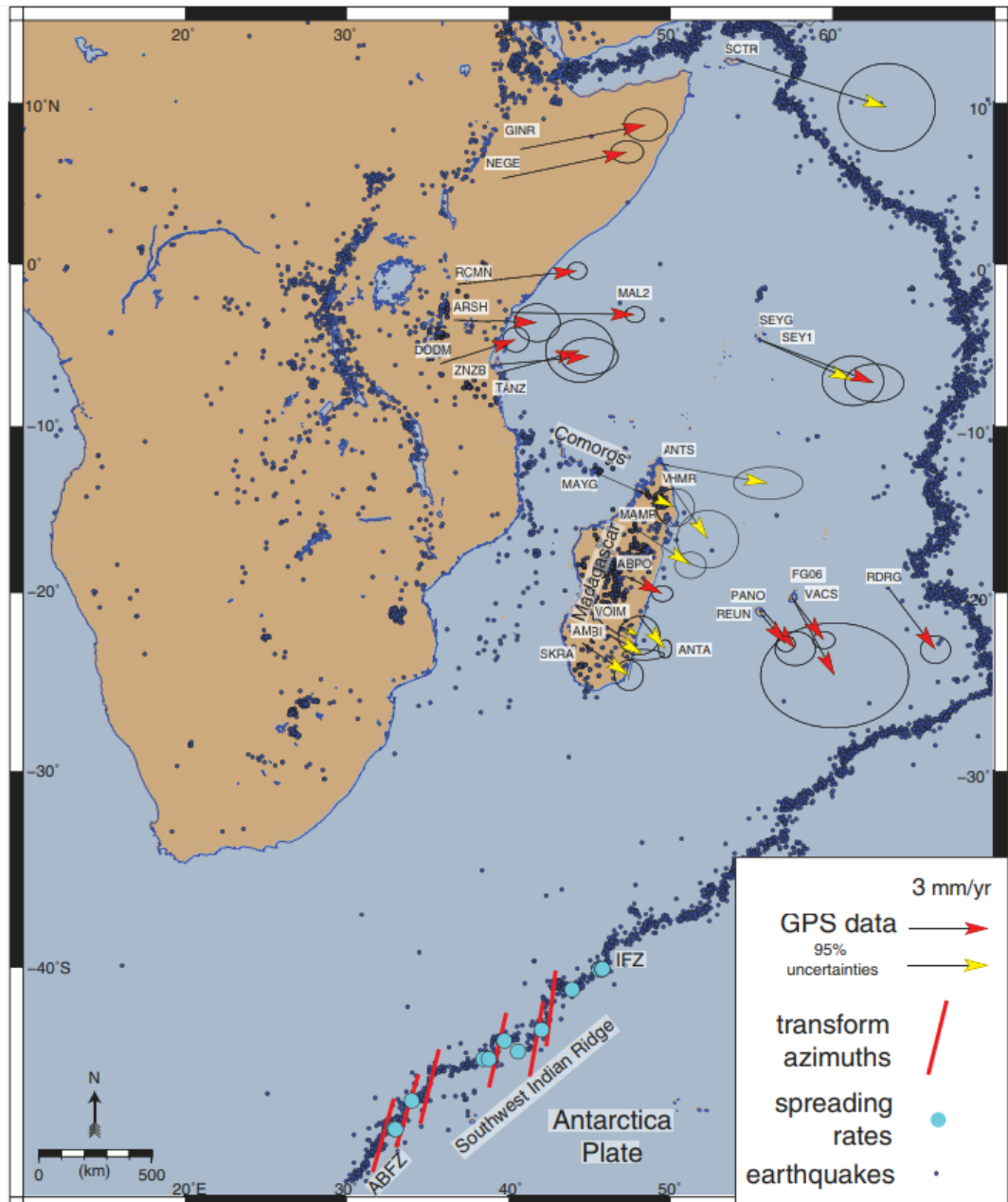


**Figure 1.** Study area (East African Rift System) with GPS station locations. Vectors represent GPS velocities in a Nubia-fixed reference frame (Saria et al., 2013). Yellow vectors represent sites that were not used in previous kinematic analyses. All uncertainties are 95%. Red bars are transform azimuths, and cyan circles indicate spreading rate data (DeMets et al., 2010). Small blue circles are seismicity data from the International Seismological Centre (2020), Lemoine et al. (2020), and Rakotondraibe et al. (2020).

## 8. 磁铁矿磁小体的热稳定性:对化石记录和生物技术的启示

翻译人: 王敦繁 dunfan-w@foxmail.com



Cypriano J, Bahri M, Kassiogé Dembelé, et al. *Insight on thermal stability of magnetite magnetosomes: implications for the fossil record and biotechnology[J]. scientific Reports, 2020, 10(1).Doi:10.1038/s41598-020-63531-5*

**摘要:** 磁小体是由磁铁矿或胶黄铁矿组成的胞内磁性纳米晶体，被趋磁细菌产生的脂质双层膜包裹。由于这些结构在细胞死亡和裂解后在某些环境中具有稳定性，磁小体磁铁矿晶体有助于沉积物的磁化，并提供了古代微生物生态系统的化石记录。磁小体在不同环境、不同条件下化学和磁性特征的保持或变化是生物技术和古地磁研究中的重要因素。在这里，我们在氧化条件下使用原位扫描透射电子显微镜评估了温度范围在 150 和 500°C 之间的磁小体的热稳定性。结果表明，磁小体在高达 300°C 的温度下是稳定的，在结构和化学上不受影响。有趣的是，样品加热到 300°C 后仍然可以观察到磁小体的膜。当加热到 300~500°C 时，在晶体中观察到腔的形成，最可能的原因是由于纳米级的克尔肯德尔效应，导致磁铁矿部分转变为磁赤铁矿。这项研究为磁小体在特定地质时期环境中的稳定性提供了一些见解，并为研究生物纳米材料提供了新工具。

**ABSTRACT:** Magnetosomes are intracellular magnetic nanocrystals composed of magnetite ( $\text{Fe}_3\text{O}_4$ ) or greigite ( $\text{Fe}_3\text{S}_4$ ), enveloped by a lipid bilayer membrane, produced by magnetotactic bacteria. Because of the stability of these structures in certain environments after cell death and lysis, magnetosome magnetite crystals contribute to the magnetization of sediments as well as providing a fossil record of ancient microbial ecosystems. the persistence or changes of the chemical and magnetic features of magnetosomes under certain conditions in different environments are important factors in biotechnology and paleomagnetism. Here we evaluated the thermal stability of magnetosomes in a temperature range between 150 and 500 °C subjected to oxidizing conditions by using in situ scanning transmission electron microscopy. Results showed that magnetosomes are stable and structurally and chemically unaffected at temperatures up to 300 °C. Interestingly, the membrane of magnetosomes was still observable after heating the samples to 300 °C. When heated between 300 °C and 500 °C cavity formation in the crystals was observed most probably associated to the partial transformation of magnetite into maghemite due to the Kirkendall effect at the

nanoscale. This study provides some insight into the stability of magnetosomes in specific environments over geological periods and offers novel tools to investigate biogenic nanomaterials.

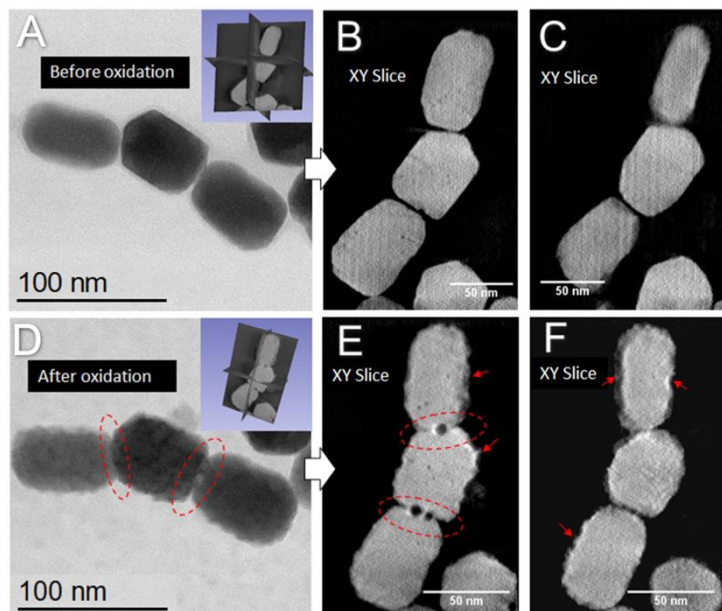


**Figure 1.** STEM image and tomography slices of a magnetosome chain before and after oxidation at 300 °C. Before: (A) BF-STEM image. Tomography performed in HAADF-STEM mode from  $-55.5^\circ$  to  $+55.5^\circ$  with a step of  $1.5^\circ$  and acquisition magnification of 800.000X. (B, C) Slices extracted from the reconstructed volume at two different depths. After: (D) BF-STEM image. Tomography performed in the same conditions as previously. (E) and (F) Slices extracted from the reconstructed volume at two different depths. The dotted ellipses in red surround nanopores formed at the interfaces between magnetite nanocrystals. The arrows point to the presence of a significant roughness at the external faces of the magnetosome.

## 9. 新仙女木冷事件气候模型模拟对比



翻译人：郑威 11930589@mail.sustech.edu.cn

Renssen H. *Comparison of Climate Model Simulations of the Younger Dryas Cold Event*[J].

*Quaternary*, 2020, 3(4): 29. <https://doi.org/10.3390/quat3040029>

**摘要：**文章比较了五个关注于气温和降水的新仙女木（YD）冷事件的气候模型模拟结果。

相对于BA间冰期，模拟显示欧洲、格陵兰岛阿拉斯加、北非、北大西洋和北冰洋海域每年都持续降温，模拟的海洋最大降温幅度在-25摄氏度到-6摄氏度之间。北美内陆的的模拟显示了更温暖的条件。在两次模拟中，南半球中高纬地区也变暖了，这与导致大西洋经向翻转环流崩溃的强烈的跷跷板效应有关。模拟的YD-BA气温响应基本上与代用指标证据一致。模拟显示所有主要的降温地区和赤道北部区域的YD-BA降水最多减少了150mm/yr。赤道以南模拟降水可能因为热带辐合带（ITCZ）的南移而增加。新仙女木事件中最大的不确定性是模型在高纬响应中呈现出不同的结果。这个不一致性可能与淡水驱动的不确定性有关。大部分模型研究都假设大西洋径向翻转环流关闭，但是这与代用指标证据不一致。

**ABSTRACT:** Results of five climate model simulation studies on the Younger Dryas cold event (YD) are compared with a focus on temperature and precipitation. Relative to the Bølling-Allerød interstadial (BA), the simulations show consistent annual cooling in Europe, Greenland, Alaska, North Africa and over the North Atlantic Ocean and Nordic Seas with maximum reduction of temperatures being simulated over the oceans, ranging from -25 °C to -6 °C. Warmer conditions were simulated in the interior of North America. In two experiments, the mid-to-high latitudes of the Southern Hemisphere were also warmer, associated with a strong bi-polar seesaw mechanism in response to a collapse of the Atlantic meridional overturning circulation (AMOC). The modelled YD-BA temperature response was in general agreement with proxy-based evidence. The simulations reveal reduced YD-BA precipitation (up to 150 mm yr<sup>-1</sup>) over all regions with major cooling, and over the northern equatorial region. South of the equator, modelled precipitation seemed to increase due to a southward shift of the InterTropical Convergence Zone (ITCZ). The largest uncertainty in the YD is the high-latitude response, where the models show diverging results. This disagreement is partly related to uncertainties in the freshwater forcing. Most model studies assume an AMOC shutdown, but this is incompatible with proxy evidence.

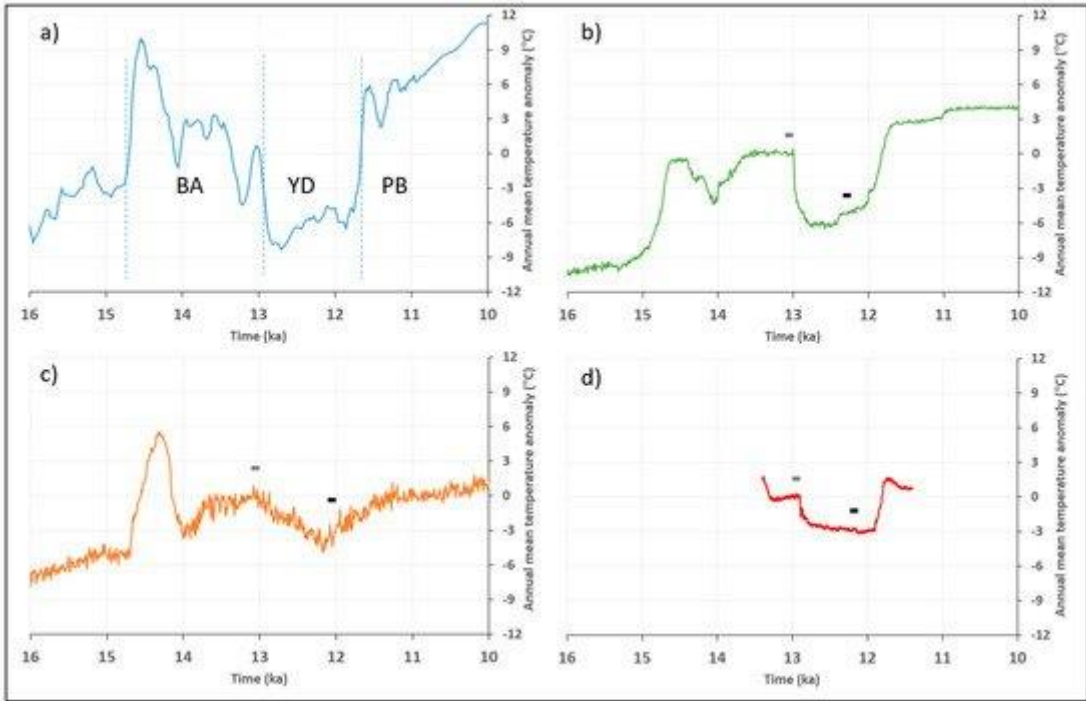


**Figure 1.** Overview of annual temperatures during the last deglaciation (16–10 ka), shown as an anomaly relative to the mean over 13.1 to 13.0 ka. (a) GISP2 ice core in central Greenland [34] provided here for reference, with BA = Bølling-Allerød, YD = Younger Dryas, PB = Preboreal. (b) DGNS experiment performed by Men viel et al. [12], (c) ALL experiment reported by He [13], and (d) COMBINED experiment by Renssen et al. [14]. The temperatures in (b–d) are for the North Atlantic Ocean and Europe in the area between  $60^{\circ}$  W– $30^{\circ}$  E, and  $40$ – $70^{\circ}$  N. Indicated are the timings of the samples for BA (small grey bar) and the YD (small black bar) discussed in this paper.

## 10. 中更新世气候过渡期中国古人类的分布和行为



翻译人：李海 12031330@mail.sustech.edu.cn

Yang, S.-X., J.-P. Yue, X. Zhou, M. Storozum, F.-X. Huan, C.-L. Deng and M. D. Petraglia. *Hominin site distributions and behaviours across the Mid-Pleistocene climate transition in China* [J]. *Quaternary Science Reviews*. 2020. 248: 106614.

<https://doi.org/10.1016/j.quascirev.2020.106614>

**摘要：**随着古人类学调查和发掘工作的不断开展，对中国早、中更新世古人类记录的了解不断增加。但气候变化对中国古人类种群的影响、对考古遗址分布和古人类行为的影响等方面的研究相对较少。中更新世气候过渡期(MPT)在东亚的时间为 1.2-0.7 Ma， 其特征是冰川-间冰期旋回的长度和强度以及季风强度和陆地条件的显著变化，这些变化与影响中国境内盆地的形成历史有关。在这里，对 MPT 期间中国各地的考古遗址分布进行了研究，以确定在这一关键时期之前、期间和之后对古人类种群潜在的长期地理和行为影响。古人类的地理分布在整个 MPT 期间都发生了变化，高纬度和低纬度地区的地点数量发生了显著变化，这可能是对变化的生态系统的响应。MPT 期间及之后，随着技术的革新，包括大型切割工具的发展，可能是对中国南方开放栖息地的形成的响应。古人类的地理和行为记录的变化，挑战了有关东亚古人类生物和文化进化的长期保守性质的传统观点，研究结果显示在早更新世和中更新世期间种群对生态系统变化的动态反应。

**Abstract:** Knowledge about the Early and Middle Pleistocene hominin record of China is steadily increasing owing to the on-going implementation of palaeoanthropological surveys and excavations. Yet, relatively little attention has been paid to the effects of climate variability on hominin populations in China and its influence on archaeological site distributions and hominin behaviours. The Mid-Pleistocene climate transition (MPT), dating to between ~1.2-0.7 Ma in Eastern Asia, is characterized by significant changes in the length and intensity of glacial-interglacial cycles and in monsoon intensity and terrestrial conditions, which have been implicated in influencing the occupation history of basins within China. Here, the MPT is examined relative to archaeological site distributions across China to determine potential long-term geographic and behavioural effects on hominin populations before, during and after this critical period. Changes in the geographic distribution of hominins are demonstrated across the MPT, with significant shifts in the number of sites in high and low latitudes, likely as a response to changing ecosystems. Technological innovations, including the development of Large Cutting Tools, occur in the MPT and afterwards, possibly a response to the formation of open habitats in South China. Geographic and behavioural

shifts in the hominin record challenge traditional views about the long-term, conservative nature of the biological and cultural evolution of hominins in Eastern Asia, and instead demonstrate dynamic responses of populations to ecosystem changes across the Early and Middle Pleistocene.

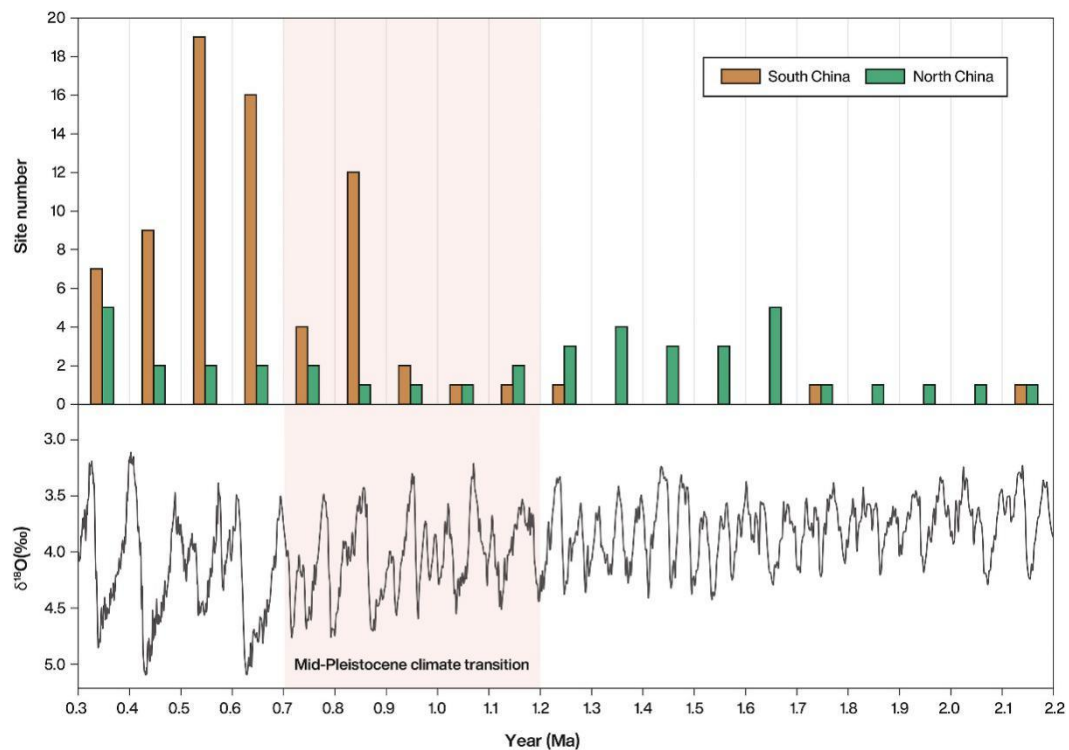


**Figure 1.** Climatic variability and site numbers in North and South China. The MPT is noted by the red vertical bar. The MPT is noted by the red vertical bar. The climate variability is based on the benthic  $\delta^{18}\text{O}$  records for ODP site 1,143 in the South China Sea

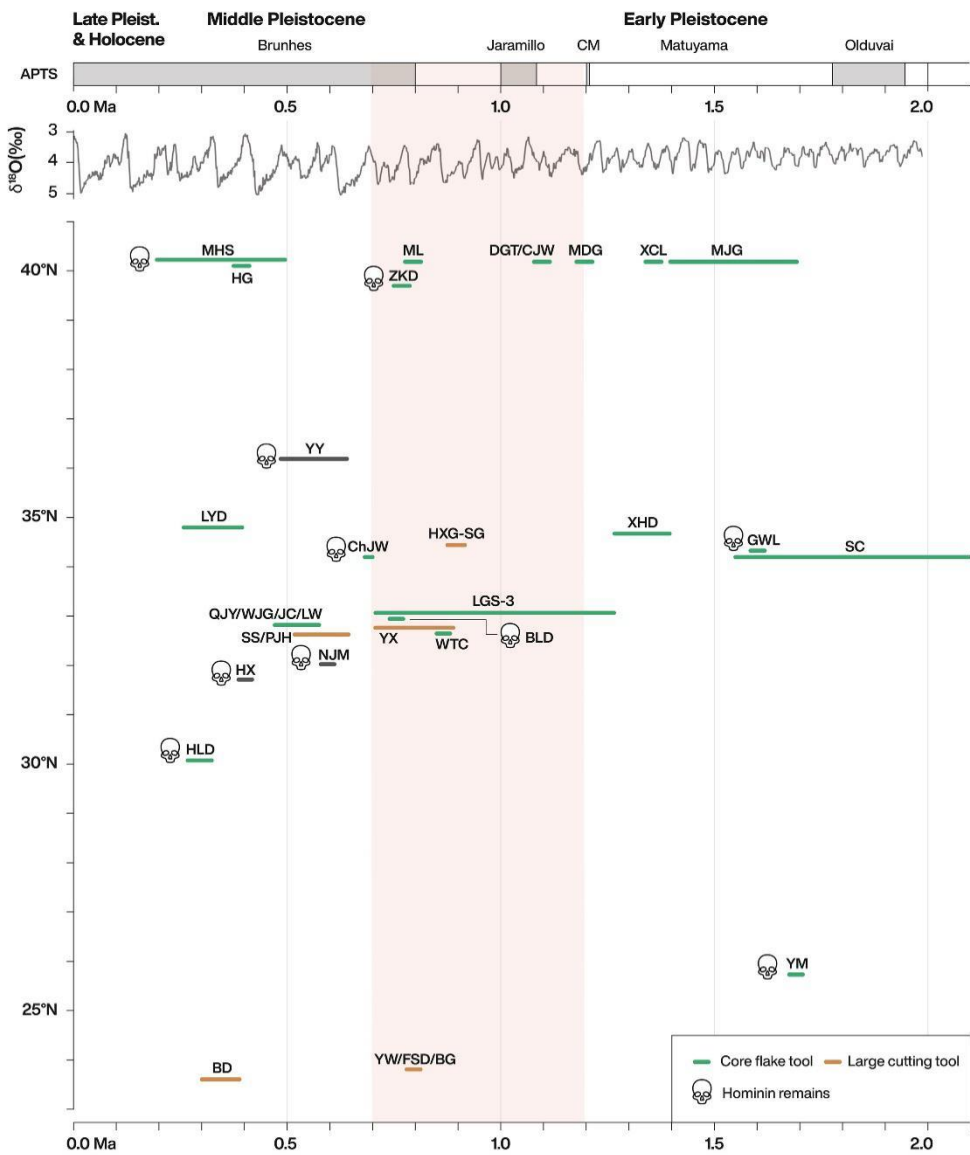


**Figure 2.** Chart displaying hominin fossils and lithic assemblages according to latitude. The orange vertical bar denotes the MPT. Benthic  $\delta^{18}\text{O}$  records for ODP Site 1143 in the South China Sea is from Tian et al., 2002. MHS: Miaohoushan, HG: Hougou, ZKD: Zhoukoudian, ML: Maliang, DGT/CJW: Donggutuo/Cenjiawan, MDG: Madigou, XCL: Xiaochangliang, MJG: Majuangou, YY: Yiyuan, LYD: Longyadong, ChJW: Chenjiawo, HXG-SG: Huixinggou-Shuigou, XHD: Xihoudu, GWL: Gongwangling, SC: Shangchen, QJY: Qiaojiayao, WJG: Wujiagou, JC: Jiuchang, LW: Liuwan, LGS-3: Longgongsi-3, BLD: Bailongdong, WTC: Wutaicun, YX: Yunxian, SS: Shuangshu, PJH: Pengjiahe, HX: Hexian, NJM: Nanjingman, HLD: Hualongdong, YM: Yuanmou, BD: Baidu, DM: Damei, YW: Yangwu, FSD: Fengshudao, BG: Baigu.

## 11. 上新世北半球冰盖因大西洋径向翻转流的增强而扩大



翻译人：张亚南 zhangyn3@mail.sustech.edu.cn

Tatsuya Hayashi, Toshiro Yamanaka, Yuki Hikasa et al., *Latest Pliocene Northern Hemisphere glaciation amplified by intensified Atlantic meridional overturning circulation* [J]. *Communications Earth & Environment*, 2020, 1:25. <https://doi.org/10.1038/s43247-00023-4>

**摘要：**自 2.7 百万年前北极冰盖扩张后，全球气候便收到冰期-间冰期旋回的控制。尽管大西洋径向翻转流对最近的气候变化表现出强烈的影响，但由于该时期北大西洋深层水形成的减弱，关于大西洋径向翻转流对北极冰盖的影响一直存在争议。通过北大西洋多种指标记录的研究。我们认为北半球冰盖的扩张受到大西洋径向翻转流加强的影响。我们发现 Iceland-Scotland Overflow Water 对北大西洋深层水的贡献在 2.7Ma 后显著增加，甚至在个别冰期的早期阶段也保持活跃，而在后期由于冰川消融而急剧减少。很有可能，冰期早期阶段北欧海域水体活跃的翻转活动促进了冰盖的有效增长以及强化冰期。

**ABSTRACT:** The global climate has been dominated by glacial – interglacial variations since the intensification of Northern Hemisphere glaciation 2.7 million years ago. Although the Atlantic meridional overturning circulation has exerted strong influence on recent climatic changes, there is controversy over its influence on Northern Hemisphere glaciation because its deep limb, North Atlantic Deep Water, was thought to have weakened. Here we show that Northern Hemisphere glaciation was amplified by the intensified Atlantic meridional overturning circulation, based on multi-proxy records from the subpolar North Atlantic. We found that the Iceland – Scotland Overflow Water, contributing North Atlantic Deep Water, significantly increased after 2.7 million years ago and was actively maintained even in early stages of individual glacials, in contrast with late stages when it drastically decreased because of iceberg melting. Probably, the active Nordic Seas overturning during the early stages of glacials facilitated the efficient growth of ice sheets and amplified glacial oscillations.

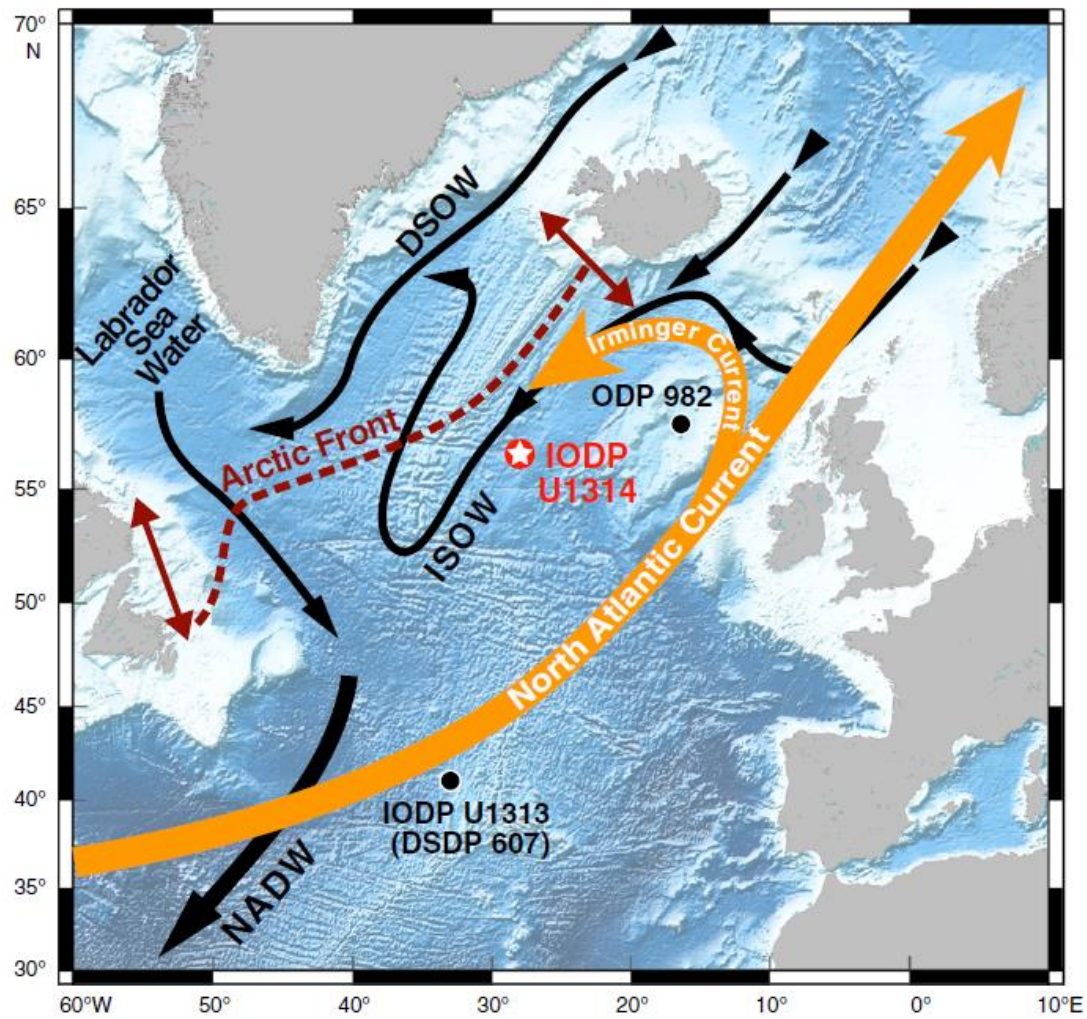


**Figure 1.** Oceanographic setting of the subpolar North Atlantic. Major ocean currents and locations of this study (IODP Site U1314,  $56^{\circ} 21.9' \text{ N}$ ,  $27^{\circ} 53.3' \text{ W}$ , water depth 2820 m) and additional deep-sea drilling sites (IODP Site U1313, Deep Sea Drilling Project [DSDP] Site 607, and Ocean Drilling Program [ODP] Site 982) discussed in the text are shown. Brown arrows denote interglacial movement of the Arctic Front.

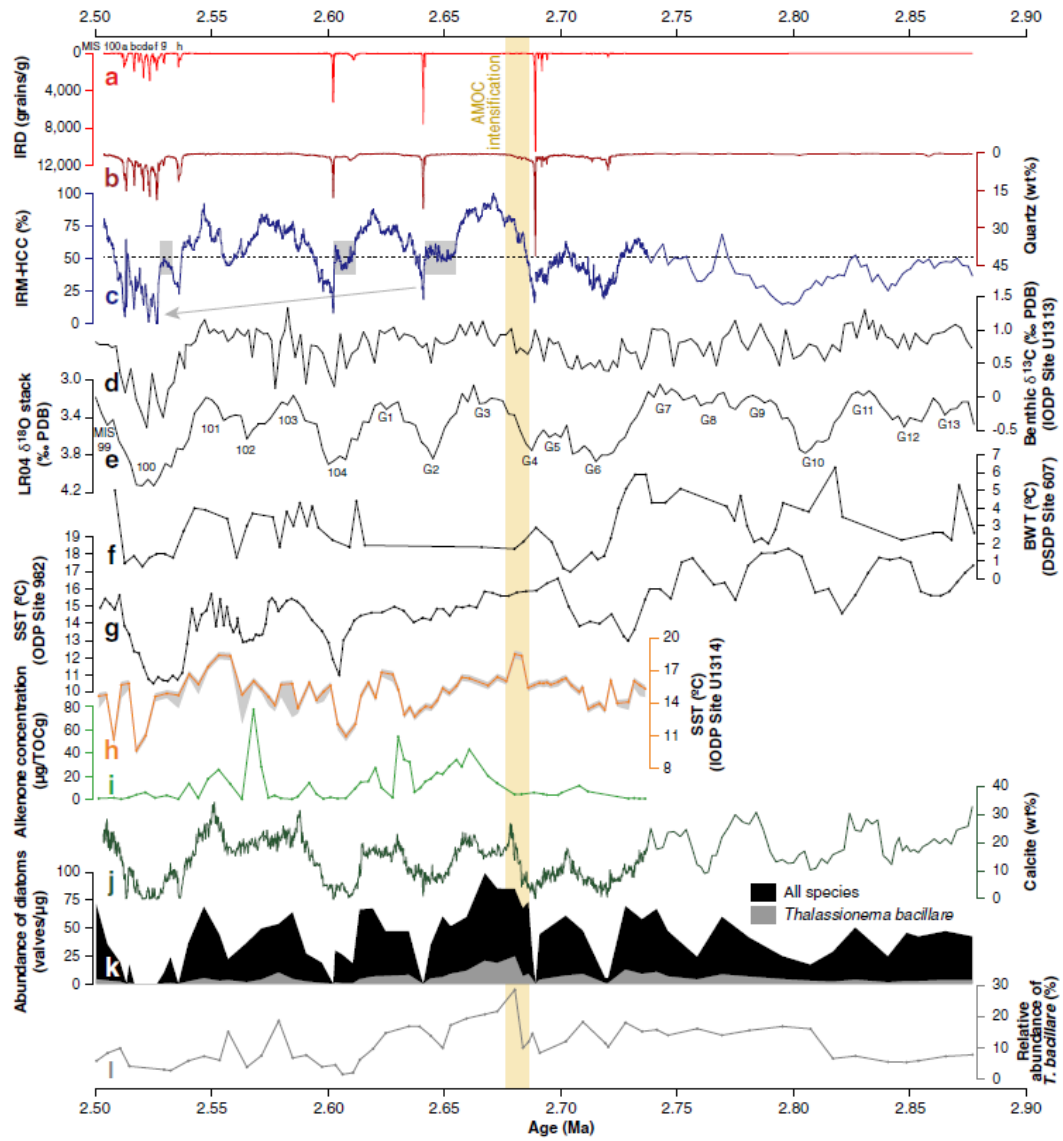


**Figure 2.** Environmental changes in the subpolar North Atlantic during the intensification of Northern Hemisphere glaciation. **a** IRD concentration (IODP Site U1314). The record between 2.54 and 2.50 Ma22 was re-analyzed in this study (see “Methods” section). Substages labeled in MIS 100. **b** Quartz weight percentage (IODP Site U1314). The record between 2.54 and 2.50 Ma22 was re-analyzed in this study (see “Methods” section). **c** HCC of IRM (IODP Site U1314). The records between 2.88 and 2.74 Ma27 and between 2.54 and 2.50 Ma22 were re-analyzed in this study (see “Methods” section). Dashed line represents an average value (0.51) calculated among the three early stages of the MIS G2, 104, and 100 glacials (gray areas). Arrow indicates a decreasing trend of the HCC in the late stages of the MIS G2, 104, and 100 glacials. **d** Benthic  $\delta^{13}\text{C}$  record reconstructed from the deep North Atlantic (IODP Site U1313)69. **e** Lisicki and Raymo (LR04) global  $\delta^{18}\text{O}$  stack. Marine isotope stages are labeled. **f** Bottom water temperature (BWT) converted from benthic foraminiferal Mg/Ca ratios (DSDP Site 607). **g** Alkenone - based SST (ODP Site 982). **h** Alkenone - based SST (IODP Site U1314). The shaded area along the estimated SST indicates the estimated error ( $0.3^\circ\text{ C}$  for positive and  $0.3^\circ\text{ C} + \text{estimated values}$  based on the injected amount of alkenones (details are shown in the “Methods” section)). **i** Alkenone concentration (IODP Site U1314). **j** Calcite weight percentage (IODP Site U1314). **k** Diatom valve concentrations of all species (black) and a warm water species, *T. bacillare* (gray) (IODP Site U1314). 1

Relative abundance of *T. bacillare* (IODP Site U1314).

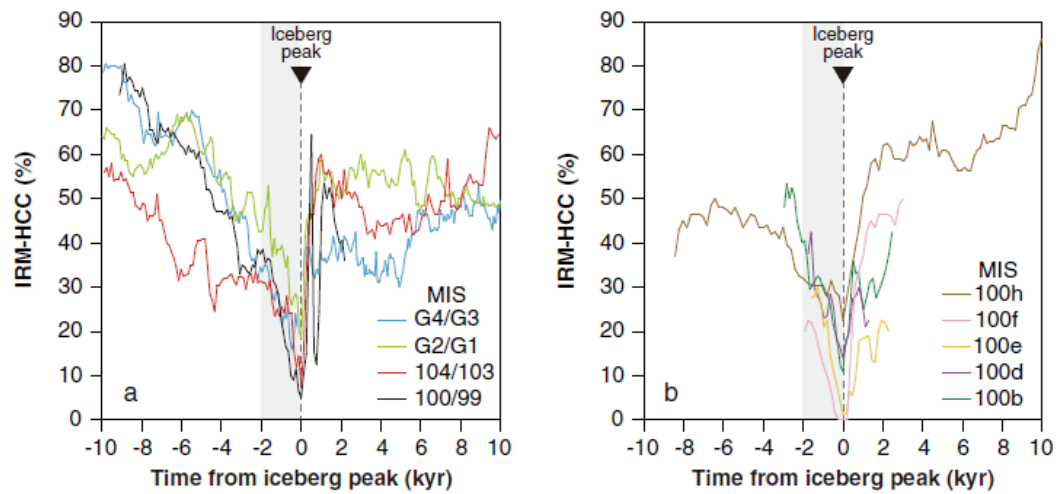


**Figure 3.** Recovery of the ISOW after the influence of large-scale iceberg melting. **a** Major deglaciations.

**b** Stadial/interstadial transitions during the MIS 100 glacial.

## 12. 非稳态成岩作用下自生亚铁磁性硫化铁的保存

翻译人：张伟杰 12031188@mail.sustech.edu.cn



Reilly BT, McCormick ML, Brachfeld SA, Haley BA. *Authigenic ferrimagnetic iron sulfide preservation due to non-steady state diagenesis: A perspective from Perseverance Drift, Northwestern Weddell Sea*[J]. *Geochemistry, Geophysics, Geosystems*. 2020.

<https://doi.org/10.1029/2020GC009380>

**摘要：**我们利用高分辨率磁化率、磁滞回线、等温剩磁获得曲线以及其他岩石磁学方法对位于南极全新世高堆积速率的生物硅酸盐洋沉积“Perseverance Drift”的一个浅的硫酸盐-甲烷过渡带(SMT)进行研究。SMT的结构通过同一岩心的孔隙水测量值确定。在SMT上部碎屑(钛)磁铁矿集合体发生溶解作用，其中化学计量磁铁矿优先溶解。高矫顽力磁性矿物溶解速度相对更慢，但是溶解作用贯穿整个SMT，可能成为孔隙水中硫酸盐消耗完之后微生物呼吸作用三价铁的来源，SMT之下孔隙水中亚铁离子的积累同样指示这个现象。在SMT超顺磁性亚铁磁性矿物的富集/消减发生在三个阶段，跟溶解的硫化物相比，溶解的亚铁与其耦合更加紧密。可以使用剩磁参数检测早期成岩作用中在SMT底部的聚集的高浓度的自生携带剩磁的含铁硫化物，如胶黄铁矿和六方磁黄铁矿。可能是SMT内持续的铁还原作用促进了含携带剩磁的的硫化铁层的形成。改变孔隙水分布的非稳态扰动(例如碳通量或沉积速率的变化)可以导致这些瞬变层的保存，就像证明孔隙水分布与海洋沉积物中氧化锰层的保存一样。

**ABSTRACT:** We document magnetic mineral diagenesis with high resolution magnetic susceptibility, hysteresis, isothermal remanent magnetization, and other rock magnetic measurements through a shallow sulfate-methane transition (SMT) at Perseverance Drift—a high-accumulation rate Holocene biosiliceous Antarctic marine sediment deposit. The structure of the SMT is defined with porewater measurements from the same core, allowing direct comparison. Dissolution of the detrital (titano)magnetite assemblage, with preferential dissolution of stoichiometric magnetite, occurs in the upper SMT. Higher coercivity magnetic minerals dissolve

more slowly, continuing to dissolve through the entire SMT and could be a source of ferric iron for microbial respiration following exhaustion of porewater sulfate, as suggested by accumulation of porewater ferrous iron below the SMT. Superparamagnetic ferrimagnetic mineral enrichment/depletion occurs in three phases through the SMT and is coupled tightly to the availability of dissolved ferrous iron relative to dissolved sulfide. High concentrations of authigenic remanence-bearing iron sulfides, including greigite and hexagonal 3C pyrrhotite, which can be detected using remanence parameters but not in-field concentration dependent parameters, accumulate in a transient horizon at the base of the SMT during this early diagenesis, where sulfide is present but limited relative to dissolved ferrous iron. Formation of this remanence-bearing iron sulfide horizon is likely facilitated by continued iron reduction through the SMT. Non-steady state perturbations that shift the porewater profile, such as changes in carbon flux or sedimentation rate, can lead to preservation of these transient horizons, much like well documented preservation of manganese oxide layers in marine sediments following similar shifts to porewater profiles.

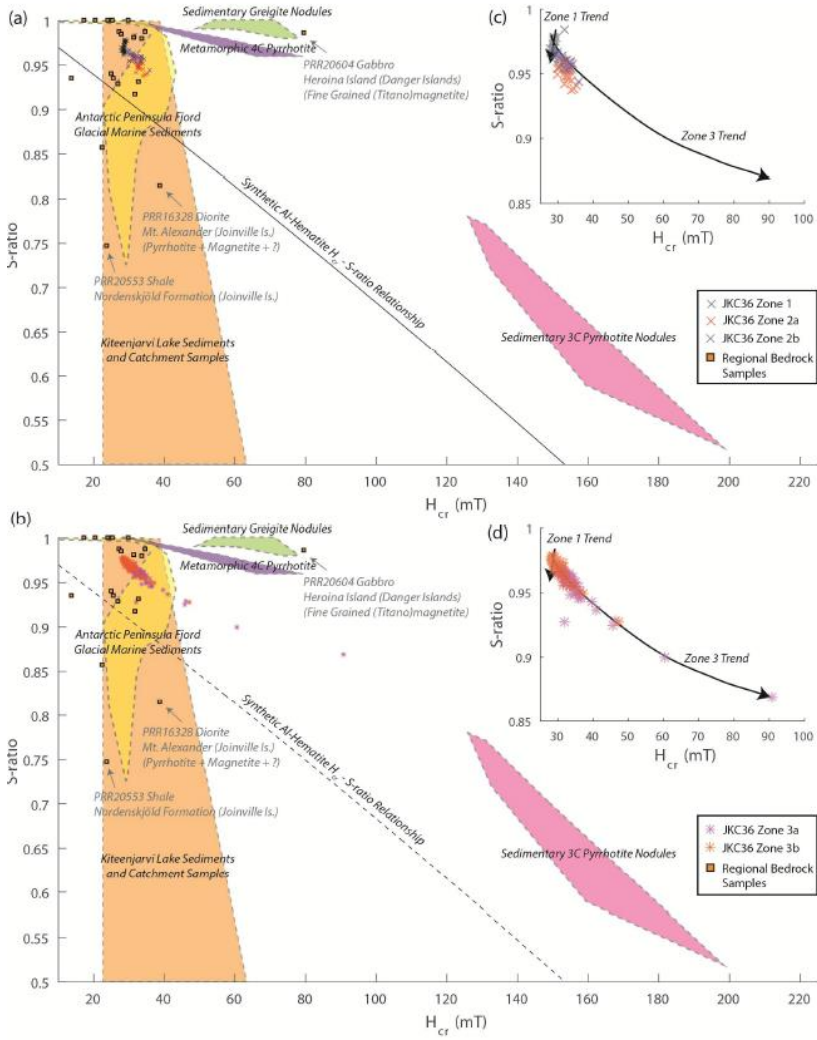


**Figure 1.** Comparison of Coercivity of Remanence ( $H_{cr}$ ) and S-ratio. Core JKC36  $H_{cr}$  and S-ratio values for (a) sulfidic sediments and (b) methanic sediments compared with regional bedrock samples (squares), values from glacial marine sediments in Barilari Bay, Western Antarctic Peninsula (yellow shading; Reilly et al., 2016), mixed hematite and magnetite magnetic mineral assemblages from Kiteenjarvi Lake and its catchment (orange shading; Stober and Thompson, 1979), and ranges for sedimentary hexagonal 3C pyrrhotite nodules (pink shading), sedimentary greigite nodules (green shading), and metamorphic rock monoclinic 4C pyrrhotite (purple shading) (Horng, 2018). The relationship between  $H_{cr}$  and S-ratio for synthetic Al-hematite samples is also plotted (black dashed line; Liu et al., 2007). (c-d) Expanded view of the Core JKC36 data, annotated with trend lines for the Zone 1 and Zone 3 samples.